Available online at www.sciencedirect.com
SCIENCE DIRECT®
Sedimentary Geology 161 (2003) 175–205
Sedimentary Geology
www.elsevier.com/locate/sedgeo

Upper Cretaceous (Campanian) phosphorites in Jordan: implications for the formation of a south Tethyan phosphorite giant

Peir K. Pufahl[a,*], Kurt A. Grimm[a], Abdulkader M. Abed[b], Rushdi M.Y. Sadaqah[b]

[a] *Department of Earth and Ocean Sciences, University of British Columbia, Vancouver, British Columbia, V6T 1Z4 Canada*
[b] *Department of Applied and Environmental Geology, University of Jordan, Amman 11942, Jordan*

Received 22 June 2001; received in revised form 14 May 2002; accepted 27 January 2003

Abstract

A record of sedimentary, authigenic, and biological processes are preserved within the Upper Cretaceous (Campanian) Alhisa Phosphorite Formation (AP) in central and northern Jordan. The AP formed near the eastern extremity of the south Tethyan Phosphorite Province (STPP), a carbonate-dominated Upper Cretaceous to Eocene ''phosphorite giant'' that extends from Colombia, North Africa to the Middle East. Multidisciplinary research of the AP and associated cherts, chalks, and oyster buildups indicate that phosphatic strata formed on a highly productive, storm-dominated, east–west trending epeiric platform along the south Tethyan margin. The onset of phosphogenesis and the accumulation of economic phosphorite coincided with a rise in relative sea level that onlapped peritidal carbonates of the Ajlun Group.

Pristine phosphates are associated with well-developed micrite concretionary horizons and contain abundant non-keeled spiral planktic foraminifera and a low diversity benthic assemblage of Buliminacean foraminifera, suggesting that pristine phosphates are a condensed facies and phosphogenesis was stimulated by the effects of a highly productive surface ocean and the suboxic diagenesis of sedimentary organic matter. The bulk sediment composition and absence of Fe-bearing authigenic phases such as glauconite, pyrite (including pyrite molds), siderite, and goethite within pristine phosphates suggests that deposition and authigenesis occurred under conditions of detrital starvation and that ''iron-pumping'' played a minimal role in phosphogenesis. Authigenic precipitation of phosphate occurred in a broad array of sedimentary environments—herein termed a ''phosphorite nursery''—that spanned the entire platform. This is a non-uniformitarian phenomenon reflecting precipitation of sedimentary apatite across a wide depositional spectrum in a variety of depositional settings, wherever the conditions were suitable for phosphogenesis.

Sedimentologic data indicate that pristine phosphates were concentrated into phosphatic grainstones through storm wave winnowing, and storm-generated, shelf-parallel geostrophic currents. Economic phosphorites formed through the amalgamation of storm-induced event beds. Stratigraphic packaging of phosphatic strata indicates that temporal variations in storm frequency were a prerequisite for the formation of economic phosphorite. Syndepositional phosphogenesis, reworking, and amalgamation to form phosphorites contrasts sharply with the principles of ''Baturin Cycling''. A transgressive systems tract coupled with high surface productivity created detritally starved settings favourable for phosphogenesis; storm reworking of pristine

* Corresponding author. Present address: Department of Geological Sciences and Geological Engineering, Queen's University, Kingston, Ontario, K7L 3N6 Canada. Tel.: +1-613-533-2599; fax: +1-613-533-6592.
E-mail address: pufahl@geol.queensu.ca (P.K. Pufahl).

0037-0738/03/$ - see front matter
doi:10.1016/S0037-0738(03)00070-8

phosphate facies produced granular phosphorite; and amalgamation of storm-generated granular event beds formed economic phosphorite in a single systems tract.

Keywords: Jordan; Phosphate rocks; Transgression; Storm sedimentation

1. Introduction

Economic phosphorites in Jordan are part of the South Tethyan Phosphogenic Province (STPP), a carbonate-dominated Upper Cretaceous to Eocene phosphorite giant that extends from Colombia, through Venezuela, North and Northwest Africa to the Middle East (e.g. Notholt, 1985; Föllmi et al., 1992). The STPP constitutes the greatest accumulation of sedimentary phosphorites known and is of considerable economic importance as it hosts 66% of the world's phosphate reserve base and accounts for approximately 30% of phosphate rock production globally (Grimm, 1997; Jasinski, 2000). These deposits accumulated on a carbonate-dominated epeiric platform along the south Tethyan margin. Like many phosphatic successions, these occurrences are also associated with biogenic carbonates and cherts.

Fascination with the STPP stems from the enormous size of the phosphorite deposits and the array of biologic and sedimentary processes that govern their stratigraphic distribution. Phosphorites contain important information regarding the physical and chemical characteristics of the ancient oceans, and provide valuable insight into the feedback processes that modify the biosphere. As one of the essential nutrients for life, P together with N governs biological productivity on Earth and thus controls the rate at which CO_2 is removed from the atmosphere and is converted into organic matter (Froelich et al., 1982; Delaney, 1998). This interaction links the P cycle to the biogeochemical cycling of C, and makes P an important regulator of the Earth's climate and ecological change over geologic time. Furthermore, the economic implications of phosphorites as a non-renewable fertilizer ore emphasize the importance of reconstructing their stratigraphic architecture, paleoenvironmental settings, and the sedimentary processes that govern their formation.

The extraordinary exposures of phosphatic and associated strata in Jordan provide an excellent opportunity to examine the paleoenvironmental factors that governed the formation of economic phosphorite in Jordan and the STPP. The purpose of this paper is to integrate sedimentologic, petrographic, paleoecologic, and stable isotopic studies of Jordanian phosphorites to: (1) elucidate the sedimentologic and authigenic conditions that prevailed over the Jordanian shelf; and (2) construct a depositional model for the formation of economic phosphorite that may be applicable to phosphatic successions elsewhere in the world.

2. Methods

The interpretations presented in this paper are based on detailed measurement and sampling of ten stratigraphic sections from Ruseifa and the northern portion of the Al Abiad/Alhisa mining districts (Fig. 1). Reconnaissance studies of phosphorite deposits in northwest Jordan and southern Al Abiad/Alhisa were also undertaken to assist with the stratigraphic correlation of phosphatic strata. The petrography of samples was studied using transmitted light microscopy complemented with back scattered electron (BSE) imaging. BSE photomicrographs and energy-dispersive X-ray spectra of specimens were acquired with a Philips XL-30 scanning electron microscope equipped with a Princeton Gamm-Tech thin-window detector. Paleocurrent analysis of selected lithofacies was done with GeoOrient v. 7, a software package for plotting stereographic projections and current rose diagrams.

Phosphatic samples intended for carbon and oxygen stable isotopic analysis of the carbonate anionic complex in carbonate fluorapatite (CFA) were first disaggregated by leaching specimens for 48 h in tri-ammonium citrate solution at pH 8.1 (Silverman et al., 1952). This treatment removes calcite but does not alter the isotopic composition of CFA (Kolodny and Kaplan, 1970; McArthur et al., 1986). Phosphatic grains were handpicked using tweezers and a dissecting microscope. Grains were then re-introduced into a solution of tri-ammonium citrate for 10 h to ensure

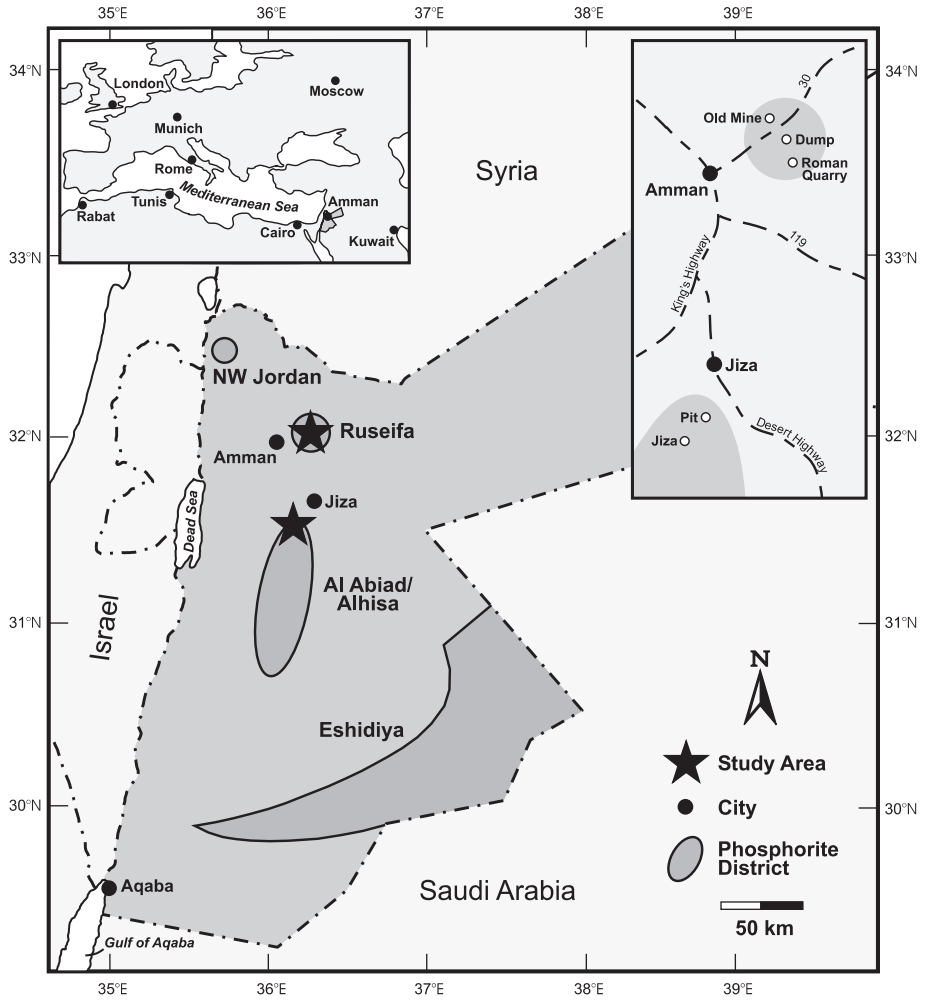

Fig. 1. Map of Jordan showing phosphorite districts, location of project area, and position of stratigraphic sections.

that all calcium carbonate had been dissolved from grain surfaces. Stable isotopic analyses were performed at the University of Western Ontario in the Laboratory for Stable Isotope Studies following the methods of McCrea (1950) using a Micromass Prism II mass spectrometer. Carbon isotopic results are reported in per mil relative to the PDB standard using the delta notation.

3. General geology

Phosphatic strata in Jordan underlie approximately 60% of the country (Abed, 1988), but economically exploitable deposits occur in only four regions: (1) NW Jordan; (2) Ruseifa; (3) Al Abiad/Alhisa; and (4) Eshidiya (Fig. 1). Together, these deposits contain an estimated 5.5 billion tonnes of mineable phosphate (Abed and Amireh, 1999; Jasinski, 2000). Phosphorites in NW Jordan, Ruseifa, and Al Abiad/Alhisa reside within the Alhisa Phosphorite Formation of the Belqa Group (Fig. 2), a 1000 m thick conformable succession of Late Coniacian to Eocene, hemipelagic chalks, cherts, micrites, and phosphorite (Bender, 1974; Powell, 1989; Sadaqah, 2000). At Eshidiya, the economic phosphorites have been interpreted by Abed and Amireh (1999) to belong to the Ajlun Group (Fig. 2) which consists of 600 m of Cenoma-

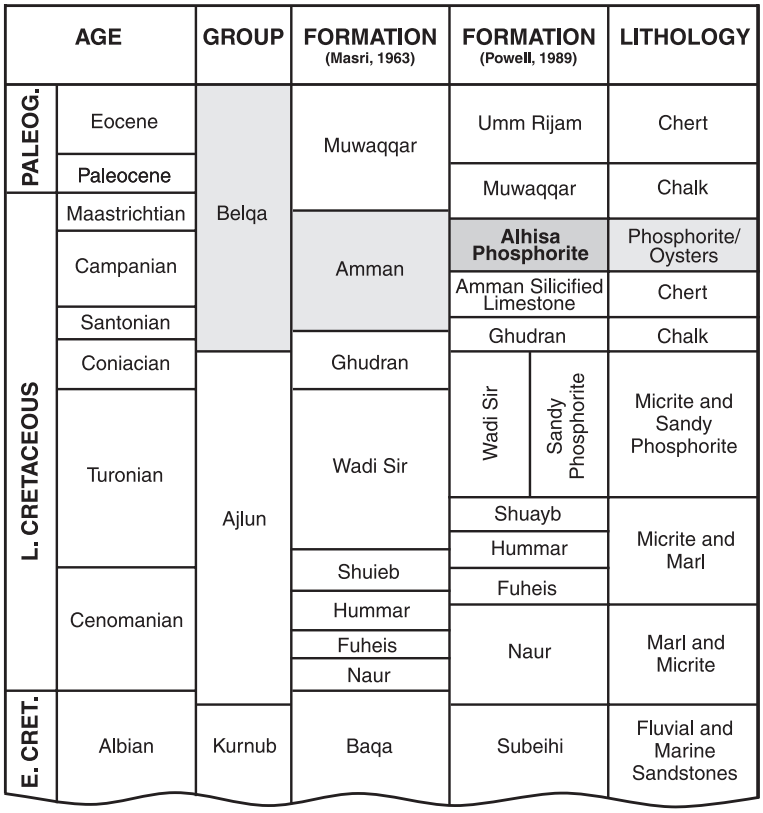

Fig. 2. Age and general lithologies within the Kurnub, Ajlun, and Belqa groups showing the stratigraphic subdivisions used by previous workers (Masri, 1963) and those used in this study (Powell, 1989). Shading denotes portion of the section studied.

nian to Turonian peritidal carbonates, cherts and chalks that disconformably underlie the Belqa Group (Bender, 1974; Powell, 1989).

The present report describes the sedimentary facies and facies associations of the Alhisa Phosphorite Formation in the Ruseifa and Al Abiad/Alhisa mining districts (Fig. 1). Consequently, only the formations within the Belqa Group are described below. Field investigations at Al Abiad/Alhisa were focused on the northern extremity of this mining district near the village of Jiza. The Alhisa Phosphorite Formation crops out within the walls of open pit mines and wadis eroded through phosphatic successions. The stratigraphic nomenclature used in this paper is that of Powell (1989).

The base of the Belqa Group is characterized by detrital chalks of the Ghudran Formation (G). This formation thins from 80 m in central Jordan to 50 m in the north, and has been determined to be Santonian in age based on ostracod-foraminifera assemblages (Bender, 1974).

The G is overlain by nearly 70 m of cherts, chalks, and micrites of the Amman Silicified Limestone Formation (ASL). The ASL thins from Al Abiad/Alhisa, where it attains a maximum thickness of 75 m, towards the north and east to 47 and 13 m, respectively. The age of the ASL has been determined by Haggart (2000) to be upper Campanian, based on the occurrence of *Baculites* cf. *ovatus*, which supports Wetzel and Morton's (1959) assignment of the ASL to the Campanian. The ASL is diachronous, younging towards the southeast (Powell, 1989).

The Alhisa Phosphorite Formation (AP) overlies the ASL and consists predominantly of interbedded phosphatic marls and granular phosphorites. The AP also thins from central Jordan in a northward direction from a thickness of 65 m at Al Abiad/Alhisa to 10 m in NW Jordan and Zakimat Al Hasah in the east of

Jordan. At Al Abiad/Alhisa the AP is divisible into three stratigraphic members, from base to top these are: the Sultani Phosphorite, Bahiya Oyster Coquina, and Qatrana Phosphorite members. Foraminifera and coccoliths indicate an upper Campanian to lower Maastrichtian age for the AP (Powell, 1989; Von Salis, written communication, 1999; Sadaqah, 2000). This is in agreement with the Campanian age of similar deposits in Egypt, Israel, and Syria (e.g. Reiss et al., 1985; Notholt et al., 1989; Glenn and Arthur, 1990). Bender (1974) has shown, based on regional mapping and field relations, that the AP is diachronous and onlaps successively younger strata towards the east and southeast.

The AP is conformably overlain by chalks of the Muwaqqar Formation (M). This formation ranges in age from the Maastrichtian to Paleocene based on planktic foraminifera and nannofossils (Bender, 1974). The M ranges in thickness from 20 to 780 m and exhibits large variations in thickness over short lateral distances (Powell, 1989).

The Umm Rijam Formation (UR) conformably overlies the M and is the uppermost unit of the Belqa Group. The UR consists predominantly of chalky limestone, chalk, and chert (Powell, 1989). Its thickness is difficult to reconstruct because its upper boundary forms the present-day erosion surface. However, there is a general trend of decreasing thickness from ~200 m in northwest Jordan to ~130 m in southern Jordan (Powell, 1989). Foraminferal assemblages indicate a Paleocene to Eocene age for the UR. The UR is not exposed within the study area.

4. Paleogeography

Economic phosphorites within the STPP accumulated at paleolatitudes between 10° and 15°N (Sheldon, 1981; Hay et al., 1999) on an east–west trending mixed carbonate–phosphorite epeiric platform along the South Tethyan margin. The common association of phosphatic strata with chert and organic-rich sediments in Israel and Egypt has been interpreted as an indication that phosphorite accumulation was associated with highly productive surface waters possibly caused by upwelling (Reiss, 1988; Shemesh et al., 1988; Almogi-Labin and Sass, 1990; Almogi-Labin et al., 1993; Kolodny and Garrison, 1994; Nathan et al., 1997).

During the Late Cretaceous the south Tethyan margin underwent periodic episodes of tectonism associated with the northward movement of the African and Arabian plates into Eurasia (Garfunkel et al., 1981; Ben-Avraham, 1989). These pulses resulted in widespread syndepositional folding of platform sediments producing an undulatory sea floor topography consisting of intrashelf sub-basins and swells (Kolodny, 1967; Reiss, 1988; Abed and Sadaqah, 1998). In the eastern Mediterranean the most pronounced of these episodes produced the Syrian Arc, an S-shaped fold belt that extends from southern Turkey into the Sinai peninsula (Freund, 1965). The Syrian Arc consists of a series of northeast to southwest trending asymmetric plunging anticlines with amplitudes of up to ~700 m and wavelengths on the order of ~20 km. Deformation along this tectonic front was contemporaneous with Upper Cretaceous phosphorite deposition, beginning in the Coniacian and continuing into the Miocene (Abed, 1988).

5. Results

5.1. Lithofacies

Fourteen lithofacies are recognised within the study area. We first describe each of these lithofacies, and then show how they are associated within the ASL, AP, and M formations. For descriptive purposes lithofacies have been arranged into three broad classes: (1) phosphatic; (2) carbonate; and (3) chert facies. The general attributes of each facies class are given in Table 1, and detailed descriptions follow.

5.1.1. Phosphatic

Three lithofacies comprise this facies class: *phosphatic marl*, *wavy laminated grainstone*, and *parallel bedded grainstone*.

5.1.1.1. Phosphatic marl. The *phosphatic marl* facies is composed predominantly of parallel and wavy, thinly laminated, reddish-orange marls that are interbedded with wavy, thickly laminated, gran-

Table 1
Characteristics and interpretation of lithofacies from the Ruseifa and Al Abiad/Alhisa mining districts

Facies category	Facies	Description	Trace fossils	Interpretation
Phosphate	Phosphatic marl	Parallel, thinly laminated chalk-rich marls interbedded with wavy, thickly laminated granular phosphatic grainstone; contain *in situ* phosphatic peloids and a poorly preserved assemblage of non-keeled, biserial and trochospiral plankic foraminifera; micrite concretionary horizons are common	Unbioturbated except when overlain by parallel bedded grainstones; facies contact bioturbated with firmground *Thalassinoides*	Hemipelagic rainout in highly productive waters; phosphogenesis, during periods of stratigraphic condensation under suboxic conditions
	Wavy laminated grainstone	Thinly laminated; laminae are fine grained, non-graded, and possess sharp lower and upper contacts; wavy laminated grainstones change laterally over several meters into poorly organised HCS grainstone sets	Unbioturbated	Deposition between fair- and storm-weather wave base under waning storm conditions
	Parallel bedded grainstones	Thickly and very thickly bedded coarse-tail graded, massive, and indistinctly stratified beds that occur separately or in tabular, 100–150 cm thick amalgamated beds; coarsest and thickest layers contain transported micrite concretions and chalk rip ups along their bases	Firmground *Thalassinoides*; micrite concretions contain simple cylindrical borings	Storm-driven transport, redeposition and amalgamation of phosphatic peloids from *phosphatic marl*
Carbonate	Chalk	Parallel laminated, massive, and bioturbated varieties; parallel laminated chalks contain *in situ* phosphatic peloids	Bioturbated chalk contains *Thalassinoides* burrow networks	Rainout of nannofossils; parallel laminated chalk, phosphogenesis, suboxic; bioturbated chalk, oxic
	Micritic limestone	Parallel bedded and massive varieties; rare coquina- and grainstone filled scours	Unibioturbated	Suspension rain of fine grained carbonate, suboxic; periodic storm scouring
	Fragmented oyster rudstone	Massive, thickly bedded oyster rudstone; forms bottomset beds to megacrossbedded oyster rudstone banks		Records bank progradation through offbank shedding
	Megacrossbedded oyster rudstone	Massive thickly bedded normally graded, oyster coquina beds organized into megacrossbedded foresets aligned 25–30° to master bedding	Endolithic borings on shell surfaces	Cascading of shell material down bank front during progradation
	Oyster framestone	Forms cores of oyster buildups and composed of large, articulated oysters in life position; forms teardrop shaped mounds that taper in a down-current direction	Endolithic borings on shell surfaces	*In situ* growth of oysters
	Chalk-rich, fragmented oyster rudstone	Chalk-rich, thickly bedded, massive, composed of oyster rudstone beds; forms topset beds that overlie oyster framestone mounds and truncates megacrossbedded oyster rudstone beds		Records stranding and storm reworking of buildup top

Table 1 (*continued*)

Facies category	Facies	Description	Trace fossils	Interpretation
	Graded oyster rudstone	Graded, thickly bedded oyster rudstone beds; intimately interbedded with chert facies	Endolithic borings on shell surfaces	Storm-induced calciclastic turbidites
	Medium bedded baculitid ammonite coquina	Consists of poorly sorted, massive and normally graded coquina beds containing abundant *Baculites* cf. *ovatus*, turritella-form gastropods, disarticulated oyster valves and crinoid fragments	Unbioturbated	Storm-induced, calciclastic turbidites derived from shallower environments
Chert	Bedded chert	Alternating beds of tan and dark-brown chert; dark-brown beds contain organic-rich blebs and form replacement seams in fractured tan cherts; pot scours common	Rare instances upper surfaces of beds contain simple cylindrical borings	Storm sweeping and silicification of carbonate-rich diatom oozes
	Chert breccia	Thin beds containing angular, pebble-sized fragments of tan chert floating in a matrix of dark-brown chert; chert fragments fit together like pieces of a jigsaw puzzle	Unbioturbated	Syneresis dessication/ auto-brecciation associated with silica diagenesis
	Chert conglomerate	Massive, medium bedded poorly sorted, sharp-based beds that contain subrounded, pebble to cobble-sized clasts of chert in matrix or clast support; intimately interbedded with bedded cherts	Pebble-sized chert clasts contain rare simple cylindrical borings	Storm reworking, transport and redeposition of bedded chert and chert breccia

ular phosphatic grainstone (Fig. 3A). In thin section parallel laminated marly laminae contain abundant *in situ*, granule-sized phosphatic peloids, silt-sized detrital quartz grains, and a poorly preserved assemblage of non-keeled, biserial and trochospiral planktic foraminifera. The poor preservation of foramanifera precludes their exact identification. Organic carbon-rich blebs are also ubiquitous throughout marly layers. The wavy laminated marls are characterized by the presence of abraded phosphatic peloids concentrated along laminae contacts.

Granular laminae consist of moderately to poorly sorted granule-sized phosphatic peloids in a chalk matrix. Slightly abraded planktic foraminifera tests, bone fragments, and pebble-sized subangular, *phosphatic marl* intraclasts are important accessory grains. Laminae have erosive bases and pinch and swell rhythmically over a lateral distance of 30–40 cm.

Discontinuous horizons of cobble-size, micrite concretions are also common within the *phosphatic marls*. Concretions are composed of calcite, and are massive oblate ellipsoids flattened in the plane of bedding that have commonly coalesced to form composite bodies 50 cm in length. Some concretions possess simple cylindrical, subvertical borings on their upper surfaces.

This facies is unbioturbated except when directly overlain by amalgamated *parallel bedded phosphatic grainstones*. In these instances the facies contact is bioturbated with well-developed *Thalassinoides* burrow networks (Fig. 3B). This facies relation occurs seven times within the logged sections and is bioturbated in every case. Traces penetrate the *phosphatic marl* to a depth of 10 cm and are passively infilled with granular phosphorite piped from overlying beds, reflecting the stable cohesive nature of the substrate at the time of colonization. *Thalassinoides* are excavated to avoid micrite concretions, suggesting a preference of the trace-maker for firm, rather than hard substrates. These features are characteristic of the *Glossifungites* ichnofacies (Pember-

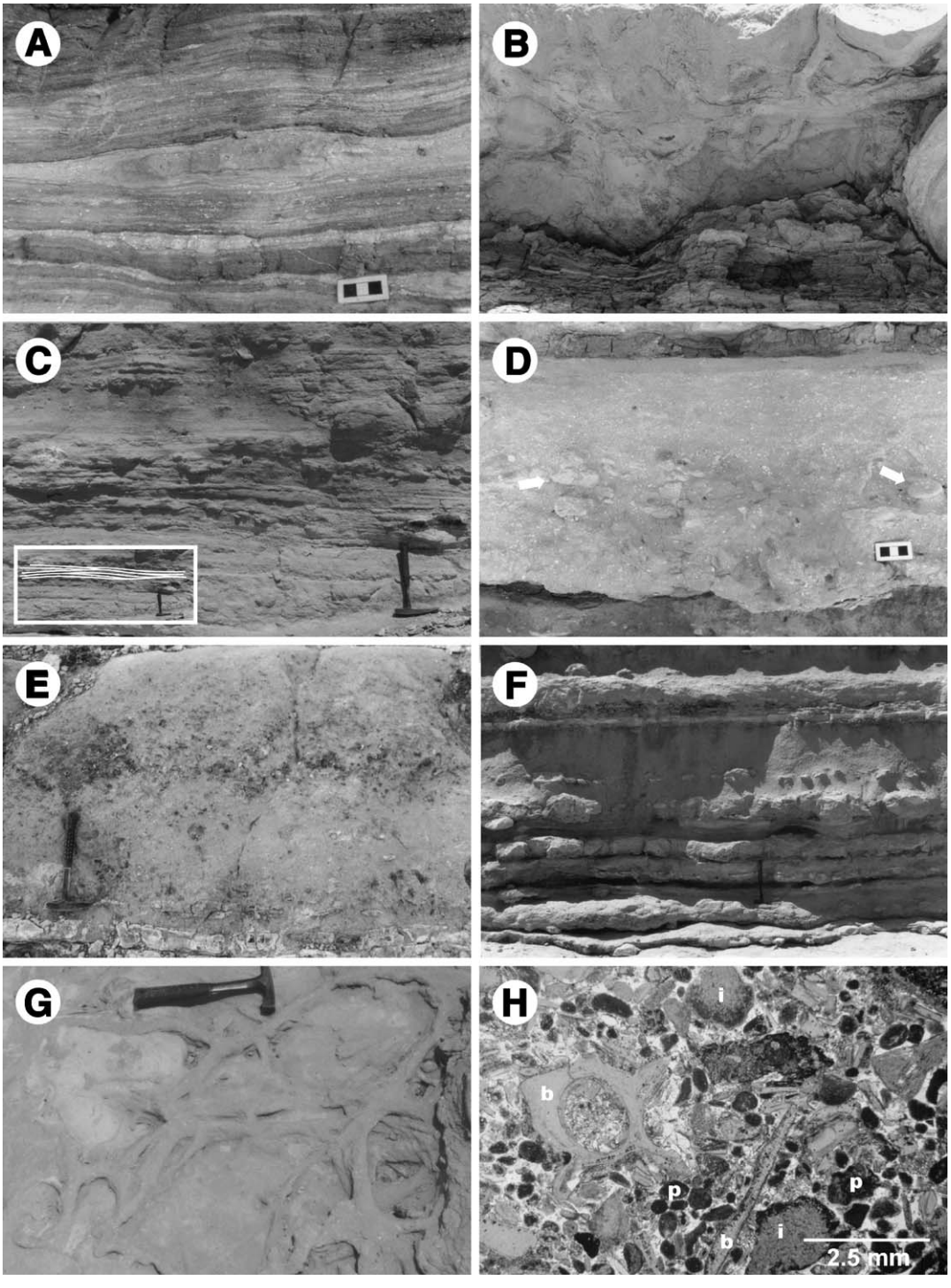
A
B
C
D
E
F
G
H
i
b
p
p
b
i
2.5 mm

ton and Frey, 1985; MacEachern et al., 1992) and record trace fossil development within semilithified or firm substrates.

Interpretation. The *phosphatic marls* are a pristine phosphate facies (Föllmi et al., 1991) where CFA precipitated authigenically *in situ*. The ubiquity of organic-rich blebs implies that this facies was originally rich in sedimentary organic matter, and the abundance of non-keeled planktic foraminifera suggests that the *phosphatic marls* accumulated beneath a highly productive surface ocean under suboxic conditions (Reiss, 1988; Almogi-Labin et al., 1993). Differential compaction around carbonate concretions and the presence of bored, reworked and transported concretions within *parallel bedded grainstones* indicates an early diagenetic origin for concretionary development at very shallow burial levels prior to significant compaction.

Sadaqah (2000) reached similar conclusions from correlative *phosphatic marls* in northwestern and south-central Jordan. These marls are also unbioturbated and have yielded low diversity assemblages of planktic and benthic foraminifera. Planktic assemblages consist primarily of *Globigerinelloides volutus*. Benthic assemblages are dominated by abundant *Bulimina* cf. *aspera* and *Neobulimina fararensis*. Almogi-Labin et al. (1993) have compared similar Upper Cretaceous planktic foraminifera assemblages from correlative strata in Israel to modern upwelling-related foraminifera populations and have shown that high abundances of *Globigerinelloides* are indicative of a highly productive photic zone. The abundance of Buliminacean foraminifera in a low diversity fauna is charactersitic of a relatively stable, dysaerobic ecosystem (Reiss, 1988; Almogi-Labin et al., 1993; Widmark and Speijer, 1997). Highly productive surface waters and the export of organic matter to the sea floor presumably created quasi-anaerobic seafloor conditions through the microbial respiration of organic matter (Pedersen and Calvert, 1990). Only specialized benthic organisms, such as Buliminacean foraminifera, can thrive under these conditions. Buliminacean assemblages have been recorded in highly productive, modern and ancient low oxygen settings from around the world (Reiss, 1988). Their common occurrence in laminated, non-bioturbated sediments like porcelanites, cherts, organic-rich carbonates, and pristine phosphates from northern South America, Morocco, Egypt, Syria, and Iraq indicate that low diversity Buliminacean assemblages (Reiss, 1988) are characteristic of Upper Cretaceous high-productivity paleoenvironments and are indicative of suboxic bottom waters.

The *phosphatic marl* facies reflects a continuum in the intensity of authigenesis and current reworking. The parallel laminated *phosphatic marls* are an unreworked pristine phosphate end-member formed from the hemipelagic rainout of phytoplankton and nannofossils. Wave-induced suspension and winnowing of the substrate produced the wavy laminated marly layers. During settling, wave oscillations apparently reached the sea floor, molding these layers into wavy laminae. As the intensity of wave reworking increased laminae became progressively more coarse-grained until granular laminae were formed from the concentration of *in situ* phosphatic peloids through winnowing.

5.1.1.2. Wavy laminated grainstone. This facies is composed predominantly of wavy laminated, fine-grained phosphatic grainstone. Laminae are non-graded and have sharp lower and upper contacts. Wavy laminated grainstones commonly change laterally over several meters into poorly organized hummocky cross-stratified grainstone sets (Fig. 3C). Laminae are composed of well-rounded, fine-grained phosphatic peloids in a chalky micritic matrix.

Fig. 3. (A) *Phosphatic marl* facies. White specs are *in situ* phosphatic peloids. Scale bar = 3 cm. (B) *Thalassinoides* bioturbated contact between *phosphatic marl* and *parallel bedded grainstone* facies. Note how the burrows are excavated to avoid the micrite concretions. (C) Field shot of the *wavy laminated grainstone* facies. The inset highlights the hummocky cross-stratification. (D) Coarse-tail graded *parallel bedded grainstone* bed with broken micrite concretions (arrows). Scale bar = 3 cm. (E) Indistinctly stratified *parallel bedded grainstone* bed. The dark band in the centre of the layer is composed of subangular, pebble-sized chert clasts and coarsens then fines upward through the thickness of the bed. (F) Amalgamated *parallel bedded grainstone* bed. Amalgamation surfaces between individual layers are demarcated by discontinuous micrite and phosphatic concretionary horizons. (G) Well-developed *Thalassinoides* burrow networks along the base of a *parallel bedded grainstone* layer. (H) Transmitted light photomicrograph of *parallel bedded grainstone*. Beds are composed of phosphatic peloids (p), phosphatic intraclasts (i), and vertebrae bone fragments (b). Phosphatic intraclasts are composed of phosphatised chalk.

Interpretation. The presence of hummocky cross-stratified phosphatic grainstone with the absence of wave-rippled reworked tops indicates that this facies accumulated between fair weather and storm wave base from suspension under waning storm conditions (Dott and Bourgeois, 1982; Duke et al., 1991).

5.1.1.3. Parallel bedded grainstones. *Parallel bedded grainstones* consist of tabular, coarse-grained, granular phosphorite beds. Beds are sharp-based, generally with planar to subplanar basal contacts and occur separately or amalgamated. Beds are either coarse-tail graded, massive, or indistinctly stratified, and are demarcated within amalgamated beds by basal scour surfaces and discontinuous phosphatic and/or micritic concretionary horizons formed at bed tops.

Coarse-tail graded beds are 1–40 cm thick and grade from a granular/pebbly base to a coarse-grained top. The thinnest beds only occur within intervals of *phosphatic marl*, where they commonly blanket micrite concretionary horizons. The coarsest and thickest beds contain abundant transported, whole and broken micrite concretions along their bases (Fig. 3D).

Indistinctly stratified beds are 40–80 cm thick and contain laterally persistent, diffuse stratification bands (Fig. 3E). Bands range in thickness from 15–30 cm, and consist of three parts: (1) a basal zone of inverse-graded granular grainstone; (2) a pebbly core composed of pebble-sized phosphatic intraclasts or sub-angular chert clasts floating in a granular matrix; and (3) a normally graded granular top. Bands do not possess distinct boundaries, but coarsen- then fine-upward gradationally over the entire layer. Massive beds range in thickness from 30–50 cm and lack internal structure.

Amalgamated *parallel bedded grainstones* are 100–150 cm thick (Fig. 3F) and are commonly bioturbated with well developed *Thalassinoides* burrow networks (Fig. 3G). Networks consist of horizontal tiers of cylindrical, bifurcating burrows infilled with granular phosphatic grainstone. Galleries are common and are developed at irregular spacings along burrows and where traces split. As in the *phosphatic marls*, burrow networks are always excavated to avoid *in situ* phosphatic and micritic concretions developed at bed tops, reflecting the development of the *Glossifungites* ichnofacies.

Grainstone beds are predominantly composed of well rounded, very coarse sand and granule-sized phosphatic peloids and sub-rounded, phosphatic intraclasts in a chalk matrix (Fig. 3H). Bone fragments and pebble-size chalk intraclasts are also common constituents within beds. Blocky calcite is the principal cement type.

Some layers are silicified and also contain angular, pebble-sized, chert rip ups. Chert rip ups are composed of microcrystalline quartz and are commonly coated with a thin isopachous calcite rim. Silicification of clasts took place selectively and incompletely, only occurring in bone fragments where the original material was replaced by microcrystalline quartz. The dominant cement types in silicified beds are equigranular microcrystalline and mosaic drusy quartz with subordinate amounts of blocky calcite. Silicification in grainstone layers occurs preferentially along layer tops, penetrating to a depth of 5–10 cm.

Interpretation. This facies represents phosphatic event beds. Normally graded beds are interpreted to have been deposited by rapid grain-by-grain deposition from suspension, with rapid burial and no significant traction transport on the bed from a single-surge, high density turbidity current (Lowe, 1982).

Massive and indistinctly stratified grainstones are interpreted to record traction carpet deposition under a sustained, turbulent current (Hiscott, 1994; Sohn, 1997). Sohn (1997) has shown that deposition from traction carpets occurs progressively from the bottom up in response to the deposition of grains at the base of the traction carpet, producing an aggraded bed whose cumulative thickness is a function of flow duration and deposition rate. Massive beds form if the grain size of the supplied sediment does not vary during deposition. However, if the grain size of the supplied sediment varies with time under sustained traction carpet sedimentation, indistinctly stratified deposits with coarsening—then fining—upward intervals with diffuse boundaries are produced. The pebbly bands within indistinctly stratified grainstone layers are interpreted to have formed in this manner, and thus record incremental aggradation of the traction carpet together with variations in the grain size and lithology of the sediment being deposited.

5.1.2. Carbonate

This facies class consists of a chalk and micrite facies, and a subgroup that includes the bioclastic carbonates.

5.1.2.1. Chalk. This facies is formed of reddish-orange, parallel laminated, massive and bioturbated chalk. The parallel laminated chalks are the most common, and consist of non-erosive, sharply based laminae. In rare instances phosphatic peloids are concentrated along the contacts between chalky laminae.

Massive chalks are similar in composition to the wavy layered chalks except for the conspicuous absence of *in situ* phosphatic peloids. Bioturbated chalks contain well developed *Thalassinoides* burrow networks identical to those within the *phosphatic marl* and *thickly bedded grainstone* facies.

In thin section the chalks are commonly recrystallized and consist of microcrystalline aggregates of silt-sized, subhedral calcite rhombs, organic carbon-rich blebs, *in situ* phosphatic peloids, and trochospiral planktic and uniserial benthic foraminifera tests (Thomas, 1999, written communication) in a calcareous nannofossil matrix.

Interpretation. The chalks were deposited by the rainout of nannofossils to the seafloor. The parallel laminated chalks are a pristine phosphate facies distinguished from the *phosphatic marls* by their higher chalk content, lower proportion of *in situ* phosphatic peloids, and the absence of associated micrite concretionary horizons. The lack of bioturbation and the ubiquity of organic-rich blebs in the laminated chalks suggest that they were initially organic-rich and may have been deposited under suboxic conditions. The presence of concentrated accumulations of phosphatic peloids along the contacts of some laminae records episodes of wave winnowing of *in situ* phosphatic peloids.

5.1.2.2. Micritic limestone. Parallel bedded micritic limestones characterize this facies. Laminae are formed of fine silt-sized aggregates of subhedral calcite rhombs and contain a poorly preserved assemblage of biserial and trochospiral planktic foraminifera and triserial benthic foraminifera (Thomas, 1999, written communication). Contacts between beds are sharp and non-erosive.

Rare, thin *parallel bedded grainstones*, scour structures (Fig. 4A), and burrowed firmgrounds are also present within this facies (Fig. 4B). Scours are scoup-shaped and infilled with either phosphatic grainstone and/or *baculitid ammonite coquina*. They are preserved as 5–10 cm long lenses with erosive soles.

Firmgrounds are sometimes reworked and best observed along facies contacts with *parallel bedded grainstones*. This facies relationship occurs 26 times and shows evidence of burrowing along the facies contact 5 times. Burrows resemble *Thalassinoides*, and are passively infilled with granular phosphorite piped from the overlying grainstone bed.

Interpretation. The parallel bedded nature and the presence of biserial and trochospiral planktic foraminifera suggests that the *micritic limestones* accumulated from suspension rain of fine-grained carbonate in an open marine environment below fair-weather wave-base. The scours within this facies closely resemble pot scours and indicate that the seafloor was periodically swept by storms. Pot scours are relatively common features of ancient storm deposits, and result from erosion by storm-induced currents flowing along an irregular seafloor (Myrow, 1992; Tsujita, 1995).

5.2. Bioclastic

The bioclastic carbonates consist of seven lithofacies, four of which comprise oyster buildups. The lithofacies that form oyster buildups will first be described and then interpreted collectively, followed by descriptions and interpretations of the remaining lithofacies.

5.2.1. Oyster buildups

Buildups are composed of four facies: (1) *fragmented oyster rudstone*; (2) *megacrossbedded oyster rudstone*; (3) *oyster framestone*; and (4) *chalk-rich, fragmented oyster rudstone*. These facies are organized into banks and isolated bioherms. Oyster banks in Jordan consist of a basal bed of *fragmented oyster rudstone* overlain by a set of *megascrossbedded oyster rudstone* that is truncated at its top by a bed of *chalk-rich fragmented oyster rudstone* (Fig. 4C). Composite banks containing stacked sets of *megacrossbedded oyster rudstone* are also present within the study area. These structures consist of a lower

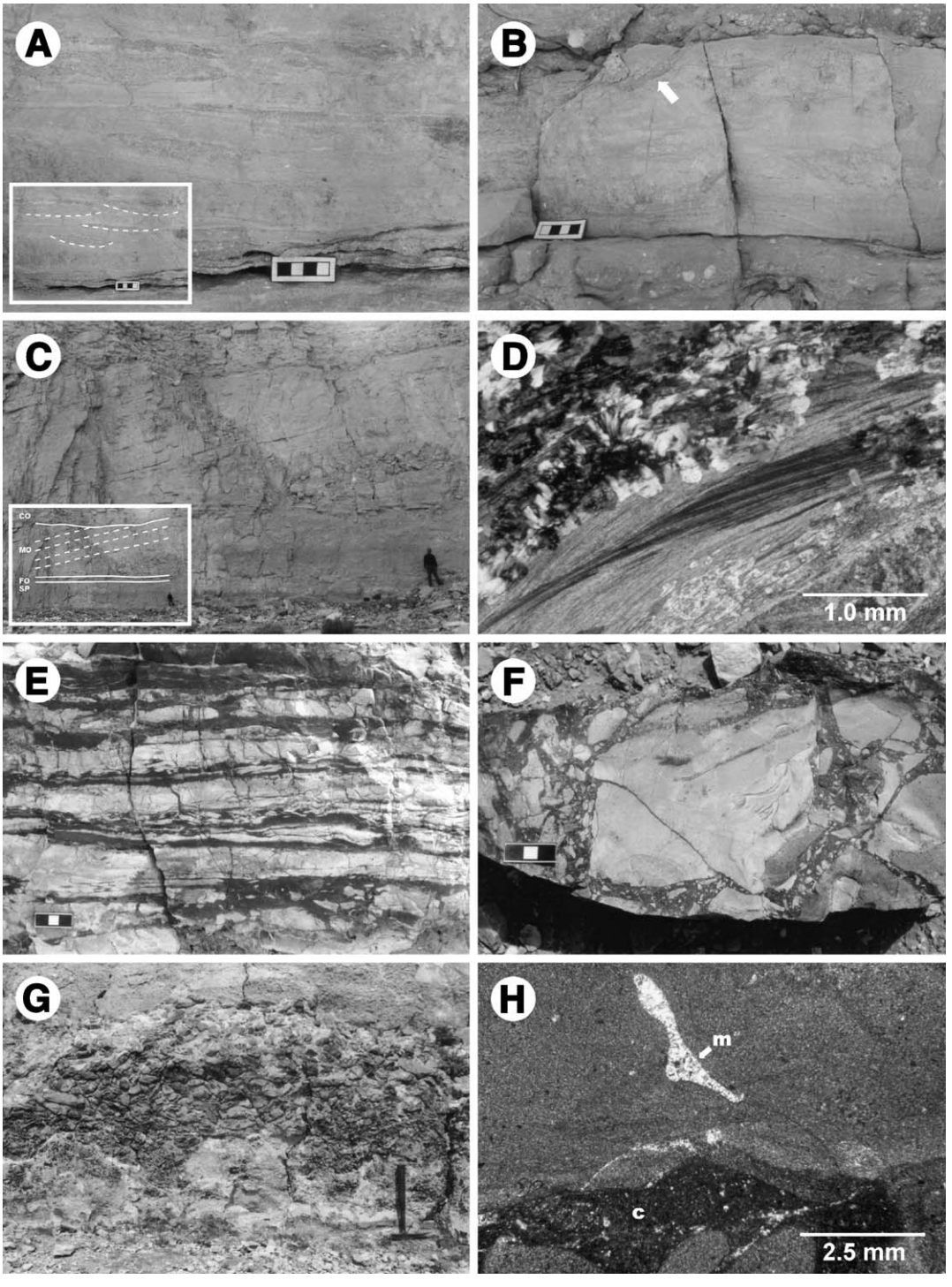
A
B
C
CO
MO
FO
SP
D
1.0 mm
E
F
G
H
m
c
2.5 mm

megacrossbedded set sharply overlain by an upper set with very different dip orientations. Banks are 8–12 m thick and pinch out laterally over several kilometres. Isolated bioherms are tear-dropped shaped and formed of an *oyster framestone* core that is flanked on its sides by *megacrossbedded oyster rudstone*. They are 6–10 m thick and extend laterally for several hundred meters. Banks and bioherms are monospecific and composed of either *Nicaisolopha nicaisei* at Ruseifa or *Ambigostrea Villei* at Al Abiad/Alhisa.

5.2.1.1. Fragmented oyster rudstone. This facies forms the base of *megacrossbedded oyster rudstone* banks. Beds are massive, range in thickness from 80–120 cm, and are composed of pebble-sized shell fragments in clast support. Individual beds show a grain size diminution in an offbank direction.

5.2.1.2. Megacrossbedded oyster rudstone. Massive and normally graded, 40–150 cm thick oyster coquina beds organized into megacrossbedded foresets constitute this facies (Fig. 4C). Graded beds contain whole and slightly abraded disarticulated oysters with rare micritic limestone rip ups at their bases, and grade gradationally to a chalk-rich top consisting of pebble-sized oyster shell fragments. Massive beds are primarily composed of disarticulated and broken oyster shells. Beds have sharp, erosive bottom contacts aligned 25–30° to master bedding.

Locally, graded and massive oyster coquina beds comprising this facies thin and become finer grained down dip over several decimetres along bank bases, changing laterally over several decimetres into *fragmented oyster rudstone*. Where several beds converge, a single thick, tabular *fragmented oyster rudstone* bed is formed that drapes the underlying strata.

Crossbed dip orientations measured from *megacrossbedded oyster rudstones* indicate that paleoflow was predominantly towards the east and south (Fig. 5). Eastward paleoflows were obtained from *megacrossbedded oyster rudstone* sets at the base of composite banks. South-directed paleocurrent directions were measured from isolated outcrops of crossbedded rudstones, and from crossbedded sets immediately above east-directed oyster rudstone sets within composite banks. The transition from east-directed to south-directed paleoflows is sharp from one set to the next.

5.2.1.3. Oyster framestone. *Oyster framestone* composes the core of oyster buildups and consists of articulated oysters in life position that form a mound in three dimensions. Shell surfaces are conspicuously microbored. Cores become progressively more chalk-rich stratigraphically upwards and commonly change laterally into poorly organized *megacrossbedded oyster rudstones*.

5.2.1.4. Chalk-rich, fragmented oyster rudstone. This facies forms beds that sharply overlie *oyster framestone* cores of buildups and truncate megacrossbedded foresets composing oyster banks (Fig. 4C). Beds range in thickness from 30 to 60 cm and are composed predominantly of pebble-sized oyster shell fragments in a chalk matrix. Pebble-sized micritic limestone rip ups and subrounded chert clasts are also common constituents within beds. Micritic limestone rip ups are plastically deformed around impinging clasts indicating that they were semilithified at the time of deposition.

In thin section unrecrystallized oyster shells from each of these lithofacies preserve a foliated structure consisting of lath-like calcite crystallites. Partially

Fig. 4. (A) Photo showing grainstone-filled scours within the *micritic limestone*. The inset highlights the base of the scours. Scale bar = 4 cm. (B) Bioturbated contact between a package of parallel bedded *micritic limestone* and an amalgamated *parallel bedded grainstone* bed. Scale bar = 4 cm. (C) Cross-section through an oyster bank showing the different architectural elements: FO—*fragmented oyster rudstone* bottomset bed, MO—foreset beds consisting of *megacross bedded oyster rudstone*, and CO—*chalk-rich, fragmented oyster rudstone* topset bed. SP—Sultani Phosphorite. Solid lines mark the contacts between elements. Dashed lines parallel the dip orientations of foreset beds within *megacrossbedded oyster rudstones*. (D) Transmitted light photomicrograph of a partially silicified oyster shell from a *megacrossbedded oyster rudstone*. Silicification within shells typically occurs preferentially along shell margins as chalcedonic replacement of the oyster calcite. (E) Photo of the *bedded chert* facies showing the alternation of tan (light gray beds) and dark brown (dark gray beds) chert beds. Scale bar = 3 cm. (F) Close-up of a typical *chert breccia* bed showing the characteristic "jig-saw" fit of tan clasts. Scale bar = 3 cm. (G) *Chert conglomerate* bed. (H) Transmitted light photomicrograph of tan (gray) and dark brown (dark gray) chert beds. Both types of beds are formed of microcrystalline chert. m—bivalve shell fragment replaced by mosaic chert. c—organic carbon-rich dark brown chert beds.

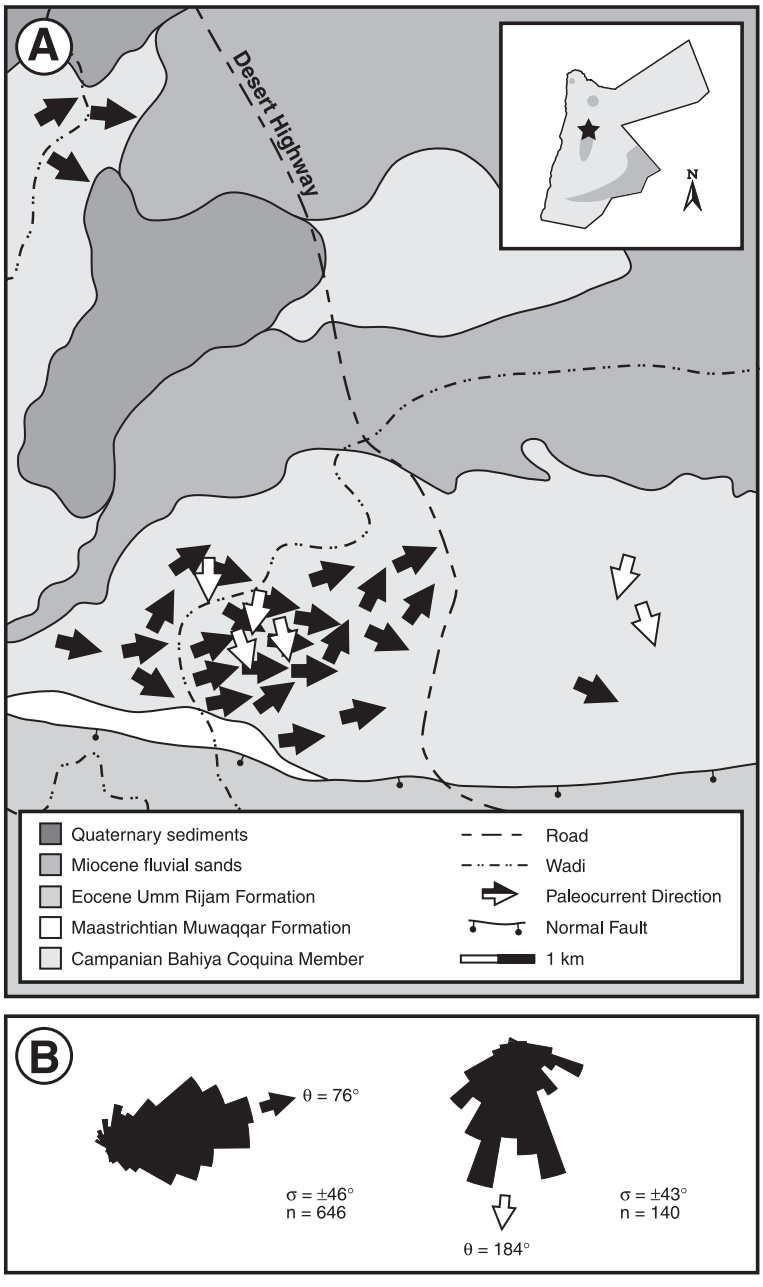

Fig. 5. Geological map with mean paleocurrent directions for the Bahiya Coquina member of the Alhisa Phosphorite Formation. Black arrows record east- and northeast-directed flow. White arrows indicate south-directed flow.

recrystallized shells have corroded margins and a patchy distribution of blocky calcite. Shells that have undergone complete recrystallization are totally replaced by blocky calcite. The matrix consists predominantly of poorly preserved calcareous nannofossils with rare, granule-sized phosphatic peloids, and ver-

tebrate bone fragments. In pervasively recrystallized beds shelter and interparticle pore spaces are completely occluded with blocky calcite.

Silicification is rare within oyster facies and when present occurs preferentially within shells and shell fragments. Silicified shells have unrecrystallized centres and are preferentially replaced along shell margins with either blocky quartz or spherulitic chalcedony, producing chert rims (Fig. 4D). In many cases these rims are in turn coated with blocky calcite. When the matrix is silicified, drusy quartz and spherulitic chalcedony are the dominant cement types. These phases are commonly overprinted by blocky calcite forming a poikiloblastic texture.

Interpretation. The *megacrossbedded oyster rudstones* are interpreted as large-scale foresets formed by the cascading of shell material in turbulent suspension down the front of oyster banks during progradation. The *highly fragmented oyster rudstone* beds are bottomset beds that record the off-bank shedding of oyster debris into distal areas. The *oyster framestones* that compose the core of bioherms developed through the *in situ* growth and accumulation of oysters. The *chalk-rich, highly fragmented oyster rudstones* are interpreted as topset beds formed by the reworking/winnowing of shell material at the top of oyster banks and isolated bioherms. This facies records the cessation of active bank progradation and bioherm growth. The teardrop shape of the oyster bioherms is controlled hydrodynamically, and suggests that unidirectional currents formed the poorly organized *megacrossbedded oyster rudstone* sets that flank the *oyster framestone core*. The vertical stacking of south-directed *megacrossbedded oyster rudstone sets* immediately over east-directed sets within composite banks indicates that progradation was dominantly towards the east and changed abruptly towards the south in the later stages of bank development.

5.2.1.5. Graded oyster rudstone. This facies consists of sharp-based, graded oyster coquina beds that range in thickness from 30–80 cm. In thin section shells are completely recrystallized and cemented with blocky calcite. This facies occurs only within intervals of *micritic limestone*, *bedded chert*, *chert breccia*, and *chert conglomerate*.

Interpretation. The *graded oyster rudstones* are interpreted to be event beds deposited from single-surge, high density turbidity currents (Lowe, 1982). The occurrence of this facies within micritic and cherty intervals suggests that *graded oyster rudstone* beds record the shedding of oyster material from oyster buildups in more proximal settings to more distal shelf environments.

5.2.1.6. Baculitid ammonite coquina. This facies is formed of poorly sorted, massive and normally graded coquina beds containing abundant *Baculites* cf. *ovatus*, turritelliform gastropods, disarticulated and abraded oyster valves, and crinoid fragments in a micritic limestone matrix (Haggart, 2000). Beds range in thickness from 10–20 cm and have sharp, erosive bases. Fossils of originally arogonitic shells consist of internal molds. This facies is commonly silicified and is intimately interbedded with micrite, *bedded cherts*, *chert breccias*, and *chert conglomerates*. Silicified shell fragments are partially or completely replaced with microcrystalline quartz and/or spherulitic chalcedony.

Interpretation. The *baculitid ammonite coquinas* are also interpreted as event strata deposited from single-surge high-density turbidity currents. The assemblage of fossil types that comprise this facies is suggestive of a shallow-water marine environment. The occurrence of *baculitid ammonite coquinas* interbedded with cherts and micritic limestones suggest that this facies was derived from more proximal shelf settings and transported offshore during storms.

5.2.2. Chert

Three kinds of chert are recognised within the study area: *bedded chert*, *chert breccia*, and *chert conglomerate*. There is a complete progression of these facies types from bedded chert to chert conglomerate that reflects the diagenetic maturation of siliceous phases, and the relative intensity of hydraulic reworking. The cherts are first described and then interpreted collectively.

5.2.2.1. Bedded chert. This facies is composed of alternating beds of tan and dark brown chert (Fig. 4E). Beds range in thickness from 1 to 3 cm and have sharp lower and upper contacts. Silicified, bored hardgrounds and *baculitid ammonite coquina*-filled scours, identical to those in the *micritic limestone*

facies, are also present within the *bedded cherts*. Tan beds are typically fractured perpendicular to bedding and pinch and swell over several decimetres. Dark-brown beds flow sympathetically around, and into fractured tan beds, forming replacement seams.

5.2.2.2. Chert breccia. This facies consists of thin beds of angular fragments of tan chert floating in a matrix of dark-brown chert (Fig. 4F). Beds are 5–10 cm thick and are confined between intervals of *bedded chert*. Contacts between brecciated horizons and *bedded cherts* are sharp, and conform sympathetically to the pinches and swells of tan chert beds above and below. Breccia fragments have sharp boundaries and fit together like pieces of a jigsaw puzzle, indicating that beds were highly competent during brecciation and underwent little or no hydraulic reworking.

5.2.2.3. Chert conglomerate. This facies consists of poorly sorted, massive chert conglomerate beds that are intimately interbedded with intervals of *bedded chert*. Beds are sharp based, range from 10–45 cm in thickness, and consist of sub-rounded to rounded, pebble to cobble-sized clasts of tan chert in both clast and matrix support (Fig. 4G).

In thin section the chert facies consist of microcrystalline quartz (Fig. 4H), and contain rare silicified trochospiral planktic foraminifera tests and bivalve shell fragments. Dark-brown cherts contain abundant organic-rich blebs and are richer in organic carbon than the tan cherts. Silicification of an originally carbonate matrix is indicated by the presence of isolated patches of unsilicified micritic limestone. Pore spaces are generally completely occluded with mosaic quartz, except in unsilicified regions where blocky calcite is the dominant cement type.

Interpretation. We interpret the chert facies to have been originally parallel bedded, carbonate-rich diatom oozes. Although siliceous microfossils are conspicuously absent within this facies, Soudry et al. (1981) have shown in correlative cherts from Israel that the origin of silica is biogenic, derived mainly from a low diversity assemblage of diatoms. The low species diversity and high abundance of diatoms within this assemblage suggests that silicification occurred in a highly productive marine setting. The absence of structures typical of subaerial exposure such as teepees, raindrop imprints, foam impressions, bubble tracks, flat-topped ripple marks, and vertebrate fossils is also internally consistent with a subaqueous origin for the chert, and indicates this facies accumulated from hemipelagic rainout below fair-weather wave-base in an open marine environment and was later silicified with remobilized biogenic silica.

The *chert breccias* are the product of *in situ* autobrecciation of the *bedded chert* facies. The splintered "jig saw puzzle" fabric that characterizes this facies indicates that the volume loss associated with the early diagenetic opal-chert transformations (Calvert, 1974; Isaacs, 1982) was apparently greater in this facies than in the *bedded cherts*. The precise origin of the breccia fabric is problematic; *in situ* subaqueous volume loss associated with syneresis is a likely explanation and is suggested by the fitted fabric (Donovan and Foster, 1972; Pratt, 1998).

The *chert conglomerate* facies is an intraformational conglomerate formed through the erosional reworking of *bedded chert* and *chert breccia* horizons. The large average grain size and the sub-rounded nature of chert clasts within this facies indicates that highly competent currents reworked the seafloor. Considering the abundant evidence for storm-generated currents in other facies, we propose that the *chert conglomerates* record episodes of intense storm reworking/winnowing of the substrate during the largest and most powerful storms.

5.3. Postdepositional processes

The ASL, AP, and M formations underwent extensive meteoric diagenesis as documented by the widespread development of blocky calcite cement, the pervasive recrystallization of shell fragments, and the poor preservation of microfossils within lithofacies. Shallow marine carbonate cements are completely absent and primary carbonate textures are best preserved within oyster shell fragments rimmed by mosaic quartz and/or spherulitic chalcedony. The common presence of intraformational chert conglomerates, the preferential silicification of the tops of grainstone beds, the development of siliceous rims on oyster shell fragments, and blocky calcite overprints on chert cements indicate that silicification occurred early, very soon after deposition near the sediment–water interface, before the meteoric alter-

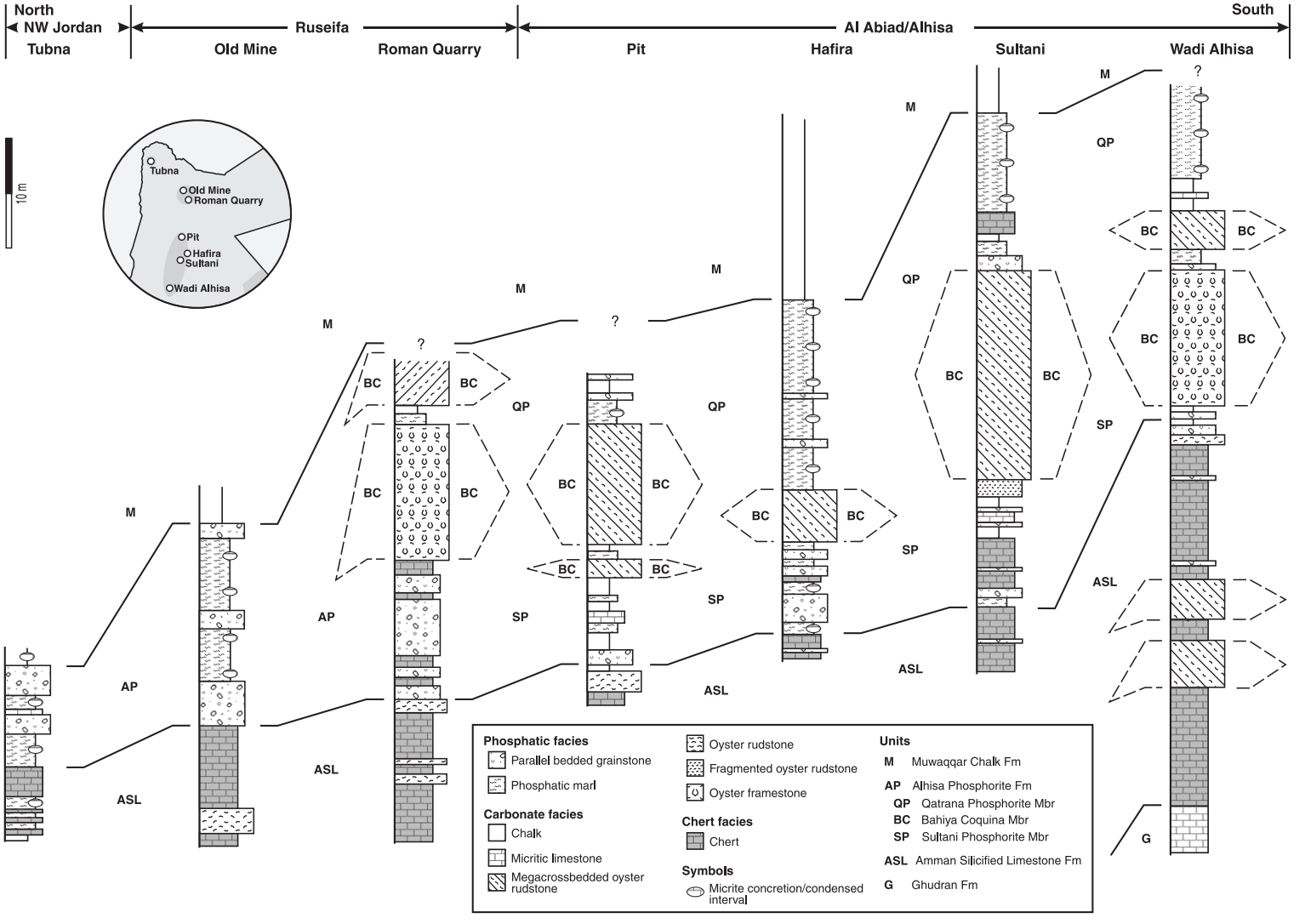

Fig. 6. Generalized fence diagram showing the regional stratigraphic framework of the Alhisa Phosphorite Formation. Sections from Tubna, Hafira, Sultani, and Wadi Alhisa have been compiled from Sadaqah (2000). Inset shows the location of the sections used to construct the fence diagram. The section is hung on the top of the Amman Silicified Limestone Formation.

ation of primary calcitic fabrics and cementation by blocky calcite.

Kolodny et al. (1980) have demonstrated based on the $\delta^{18}O$ signature and B content of remarkably similar cherts in Israel, that the fractured and brecciated textures of the cherts are the product of remobilization of biogenic silica in a two-stage silicification process. In the Israeli cherts, the first phase of silicification occurred soon after deposition in a normal marine environment, and resulted in the selective silicification and autobrecciation of organic-poor carbonate mudstones that produced chert breccias enriched in both ^{18}O and B. The second stage occurred after initial brecciation and records the silicification of organic-rich carbonate mudstones within meteoric waters that were depleted in ^{18}O and B. This phase of diagenesis was evidently driven by the equilibration of the tan cherts with fresh water at shallow burial levels.

The selective silicification observed within the Jordanian cherts is thought to reflect the compositional differences between organic-rich and organic-poor carbonate mudstone beds. The presence of organic matter and clay has been shown to inhibit the rate of silicification (Isaacs, 1982; Hinman, 1990; Behl and Garrison, 1994), whereas calcium carbonate accelerates chert formation by increasing the rate of diagenetic opal nucleation (Greenwood, 1973; Isaacs, 1982). These findings are in keeping with what is observed within chert facies, that silicification first occurred during early diagenesis within carbonate mudstones barren of organic matter. We postulate that only when the sediments were exposed to, and equilibrated with meteoric waters did the organic-rich carbonate mudstones begin to silicify.

5.4. Regional stratigraphy

The sedimentary facies described above occur in three natural associations that reflect the range of sedimentary processes that occurred over the Jordanian shelf. These groupings correspond to the ASL, AP, and M formations and form a fining upward succession that suggests continuous, conformable depositional evolution during the accumulation of economic phosphorites. The regional stacking pattern of peritidal carbonates of the Ajlun Group overlain by hemipelagic cherts, phosphorites, and chalks of the Belqa Group indicate that the ASL, AP, and M were deposited during a rise in relative sea level and constitute the upper portion of a transgressive systems tract. Fig. 6 shows the lithofacies associations within the ASL, AP, and M on a regional scale in a north–south transect through the NW Jordan, Ruseifa, and Al Abiad/Alhisa mining districts. These facies relations are described below.

Where the ASL crops out within the study area it is distinguished by the ubiquitous presence of chert, and consists of *bedded chert*, *micritic limestone* interbedded with *chert breccia, chert conglomerate*, *baculitid ammonite coquinas*, *graded oyster rudstone beds*, and *thickly bedded phosphorite* beds. The alternation of lithofacies is the most striking feature of this formation.

The AP consists of interbedded oyster build-ups and phosphatic facies in central Jordan, and is divisible into the Sultani Phosphorite, Bahiya Coquina, and Qatrana Phosphorite members (Fig. 6). It thins laterally towards the north where it is composed of alternating intervals of amalgamated beds of *parallel bedded grainstone* and *phosphatic marl*. The alternation of intervals of pristine phosphate and granular phosphorite is also recognized in correlative deposits in south-central Jordan (Abed and Sadaqah, 1998), Iraq (Al-Bassam et al., 1983), Israel (Nathan et al., 1979; Soudry and Champetier, 1983), and Egypt (El-Kammar et al., 1979; Glenn, 1990). The AP is characterized by the ubiquitous presence of micrite concretionary horizons within phosphatic facies throughout its entire thickness. Where the M is exposed within the study area it consists of *chalk* with thin packages of *phosphatic marl*.

6. Interpretation and discussion

6.1. Phosphogenesis

Primary phosphogenesis is the process of CFA precipitation (generally as francolite—$Ca_{10-a-b}Na_aMg_b(PO_4)_{6-x}(CO_3)_{x-y-z}(CO_3{\cdot}F)_{x-y-z}(SO_4)_zF_2$) within the upper few centimetres of sediment (Jahnke et al., 1983; Froelich et al., 1988; Jarvis et al., 1994). Phosphogenesis is a biogeochemical process governed by microbially mediated Eh and pH of bottom and pore waters, dissolved chemical species, and sedimentation rates (Föllmi et al., 1991). It is distinct from the hydraulic and biological reworking and/or winnowing processes that concentrate phos-

Table 2
Isotopic data

Phosphorite District	Sample Number	Lithofacies	$\delta^{13}C$ (PDB)	Reference
NW Jordan	T-1	Phosphatic marl	− 7.50	[2]
	T-3d	Phosphatic marl	− 6.55	[2]
	T-9	Phosphatic marl	− 7.31	[2]
	T-21	Phosphatic marl	− 9.37	[2]
	T-23	Phosphatic marl	− 11.18	[2]
	T-33	Phosphatic marl	− 8.65	[2]
	Z-3	Phosphatic marl	− 3.02	[2]
	J-7	Phosphatic marl	− 8.38	[2]
	J-21	Phosphatic marl	− 3.49	[2]
	K-1	Phosphatic marl	− 6.18	[2]
	K-3	Phosphatic marl	− 2.42	[2]
	K-9	Phosphatic marl	− 7.79	[2]
	K-11	Phosphatic marl	− 5.45	[2]
	K-15	Phosphatic marl	− 4.72	[2]
	K-21	Phosphatic marl	− 4.29	[2]
Ruseifa	OM-5	Parallel bedded grainstone	− 9.03	[1]
	OM-18	Wavy laminated chalk	− 8.19	[1]
	OM-16A	Phosphatic marl	− 11.59	[1]
	OM-27	Phosphatic marl	− 11.21	[1]
	RQ-1	Parallel bedded grainstone	− 7.95	[1]
	DJ-35	Parallel bedded grainstone	− 8.96	[3]
	DJ-40	Parallel bedded grainstone	− 9.36	[3]
	DJ-47	Parallel bedded grainstone	− 7.97	[3]
	DJ-51	Parallel bedded grainstone	− 6.21	[3]
	DJ-52B	Parallel bedded grainstone	− 5.67	[3]
	ASP-8	Parallel bedded grainstone	− 9.9	[4]
	ASP-9	Parallel bedded grainstone	− 8.9	[4]
Northern Al Abiad/ Alhisa	Q-4	Parallel bedded grainstone	− 7.53	[1]
	Q-20	Phosphatic marl	− 6.24	[1]
Southern Al Abiad/ Alhisa	W-30	Phosphatic marl	− 5.45	[2]
	W-43	Phosphatic marl	− 2.36	[2]
	W-46	Phosphatic marl	− 8.42	[2]
	W-49	Phosphatic marl	− 6.19	[2]
	S-9	Phosphatic marl	− 5.82	[2]
	S-15	Phosphatic marl	− 8.00	[2]
	S-17	Phosphatic marl	− 6.74	[2]
	S-22	Phosphatic marl	− 7.19	[2]
	S-23	Phosphatic marl	− 7.26	[2]
	F-13	Phosphatic marl	− 3.63	[2]
	F-15	Phosphatic marl	− 2.20	[2]
	F-16	Phosphatic marl	− 6.89	[2]
	F-18	Phosphatic marl	− 3.21	[2]
	F-20	Phosphatic marl	− 5.66	[2]
	DJ-61B	Parallel bedded grainstone	− 5.91	[3]
	DJ-64	Parallel bedded grainstone	− 10.44	[3]

[1]—This study; [2]—Sadaqah (2000); [3]—McArthur et al. (1986); [4]—Shemesh et al. (1983).

phatic sediments into economic phosphorites (Baturin, 1971; Glenn et al., 1994).

In many modern environments phosphogenesis frequently occurs beneath the sites of active upwelling along the west coasts of South America, Baja California, southern Africa, and India (Glenn et al., 1994). In these regions intense coastal upwelling provides a supply of nutrients to surface waters, resulting in high primary productivities, and high organic carbon fluxes to the seafloor. The precipitation of CFA within these settings is stimulated by the production of pore water phosphate generated through the microbial degradation of organic matter (Burnett, 1977; Froelich et al., 1983; Jahnke et al., 1983), and the dissolution of fish bones (Suess, 1981). CFA precipitated within these environments has very distinctive $\delta^{13}C$ signatures (Irwin et al., 1977), and is distinguished by having a significant portion of their carbon derived from microbially degraded organic carbon.

The range of $\delta^{13}C$ (CO_3-CFA) values shown in Table 2 in comparison with modern pore water total dissolved $\delta^{13}C$ values from anoxic sediments and from other ancient deposits (McArthur et al., 1980, 1986; Benmore et al., 1983; Shemesh et al., 1983; Glenn and Arthur, 1990; McArthur and Herczeg, 1990; Compton et al., 1993) suggests that phosphatic grains from the *phosphatic marls*, *chalks*, and *parallel bedded grainstones* precipitated under conditions of sulfate reduction (Table 3; Froelich et al., 1979). These data also indicate that the *parallel bedded grainstones* were derived through the hydraulic concentration of phosphatic peloids from the *phosphatic marls* and wavy laminated chalks, and further supports the sedimentologic and microfossil data suggesting that pristine phosphates are a dysaerobic facies.

Table 3
Stepwise microbial respiration of organic matter (CH_2O) and change in the $\delta^{13}C$ signature of marine pore water with downward decreasing metabolic energy yields (after Froelich et al., 1979; Glenn and Arthur, 1990)

TDC $\delta^{13}C$	Redox state	Oxygen (m/l)	Diagenetic zone	Reaction
From: ± 0.5 ‰ (bottom water)	oxic	8.0–2.0	aerobic oxidation	$CH_2O + O_2 \rightarrow CO_2 + H_2O \rightarrow HCO_3^- + H^+$
	suboxic	2.0–0.0	manganese reduction	$CH_2O + 3CO_2 + H_2O + 2MnO_2 \rightarrow 2Mn^{2+} + 4HCO_3^-$
			nitrate reduction	$5CH_2O + 4NO_3^- \rightarrow 2N_2 + 4HCO_3^- + CO_2 + 3H_2O$
			ferric iron reduction	$CH_2O + 7CO_2 + 4Fe(OH)_3 \rightarrow 4Fe^{2+} + 8HCO_3^- + 3H_2O$
	anoxic	0.0	sulphate reduction	$2CH_2O + SO_4^{2-} \rightarrow H_2S + 2HCO_3^-$
To: −25 ‰			methanogenesis	$2CH_2O \rightarrow CH_4 + CO_2$
To: +25 ‰				

TDC = total dissolved carbon in pore water.

The intimate association of the *phosphatic marls* with well developed micrite concretionary horizons and firmground *Thalassinoides* suggests that precipitation of CFA was associated with periods of stratigraphic condensation. Sedimentologic and stable isotopic studies of similar concretionary horizons in the Miocene Monterey Formation, California (Garrison and Graham, 1984; Baker and Burns, 1985; Compton and Siever, 1986), the Oligo-Miocene Timbabichi Formation, Baja California Sur (Grimm, 2000), the Lower Jurassic Jet Rock, England, and the Middle Jurassic Opalinus mudstone, Switzerland (Wetzel and Allia, 2000) show that concretions form at shallow burial levels during periods of low net sedimentation. These "hiatal" concretions typically record a multiphase growth history that includes repeated episodes of concretion exhumation, boring and/or encrustation, transport/redeposition, and continued concretion growth through the precipitation of additional cement. They precipitate at or near the sediment–water interface within a zone of high alkalinity generated by the microbial respiration of sedimentary organic matter. The fixing of this zone at shallow burial levels during periods of arrested sedimentation thus favours carbonate precipitation by preconditioning pore waters with the necessary solution and surface chemistries for extended periods of time (e.g. Baker and Kastner, 1981; Baker and Burns, 1985; Compton et al., 1994). In terms of sequence stratigraphy, these concretionary horizons are genetically linked to sediment starvation associated with a rise or highstand in relative sea level (Grimm, 2000; Wetzel and Allia, 2000).

Low net sedimentation rates also promote phosphogenesis by allowing high concentrations of pore-water phosphate and fluoride (Föllmi et al., 1991). The precipitation of CFA is favoured by a high pH and is restricted to shallow burial levels by the diffusion of F from seawater (Jahnke et al., 1983; Glenn and Arthur, 1988). In Jordan, changes in this relationship between sedimentation rate and phosphogenesis are manifested as a continuum in the proportion of *in situ* phosphatic peloids within pristine phosphate facies, and in the stratigraphic density of associated micrite concretionary horizons; the higher the degree of stratigraphic condensation the greater the level of authigenesis. The *phosphatic marls* have the highest concentration of *in situ* peloids and density of micrite concretionary horizons, and are thus interpreted to record the lowest net sedimentation rates. The relatively low concentration of phosphatic peloids and the absence of micrite concretionary horizons within the parallel laminated chalk reflect the relatively high rates of sedimentation associated with chalk deposition (Zijlstra, 1995).

Sedimentologic data also indicate that iron redox pumping of pore water phosphate likely played a minimal role in phosphogenesis. Iron redox pumping is a cyclic mechanism that enriches phosphate in pore waters by the release of phosphate sorbed onto iron oxyhydroxides in organic lean sediments (Froelich et al., 1988; Heggie et al., 1990; Schuffert et al., 1998). It is dependent upon the availability of iron within the sediments and is important in promoting phosphogenesis in areas that are not associated with prominent upwelling. The association of phosphorite with glauconite and/or interbedded siliclastics that is common in some phosphogenic systems, including correlative phosphatic sediments from the Mishash Formation in Israel (Soudry, 1992) and the Duwi Group phosphor-

ites in Egypt (Glenn, 1990), is not recognized within the study area. The conspicuous absence of mudrocks and shales, and the lack of glauconite and other Fe-bearing authigenic phases such as pyrite (including pyrite molds), goethite, and siderite within phosphorites from central and northern Jordan is a defining feature and sets them apart from their Israeli and Egyptian counterparts. The precipitation of Fe-bearing authigenic minerals is controlled largely by the availability of detrital iron within the sediments and may exist only in siliciclastic dominated phosphogenenic environments. Detrital sediments on the Jordanian shelf were trapped in more proximal settings during marine transgression, thereby starving mid and distal platform environments of a source of iron. Consequently, Fe-bearing authigenic minerals did not form. Phosphogenesis is thus inferred to have been stimulated primarily by the microbial respiration of sedimentary organic matter derived from a highly productive surface ocean.

6.2. Depositional model

The characteristics of individual lithofacies and their associations within the ASL, AP, and M indicate that deposition occurred conformably on a highly productive, east–west trending epeiric platform (Fig. 7). The ubiquitous presence of chert and the abundance of non-keeled, trochospiral planktic foraminifera are suggestive of high levels of primary productivity (Soudry et al., 1981; Reiss, 1988; Amolgi-Labin et al., 1993; Thomas, 1999, written communication). The ASL, AP, and M are analogous to the facies belts that develop in several modern

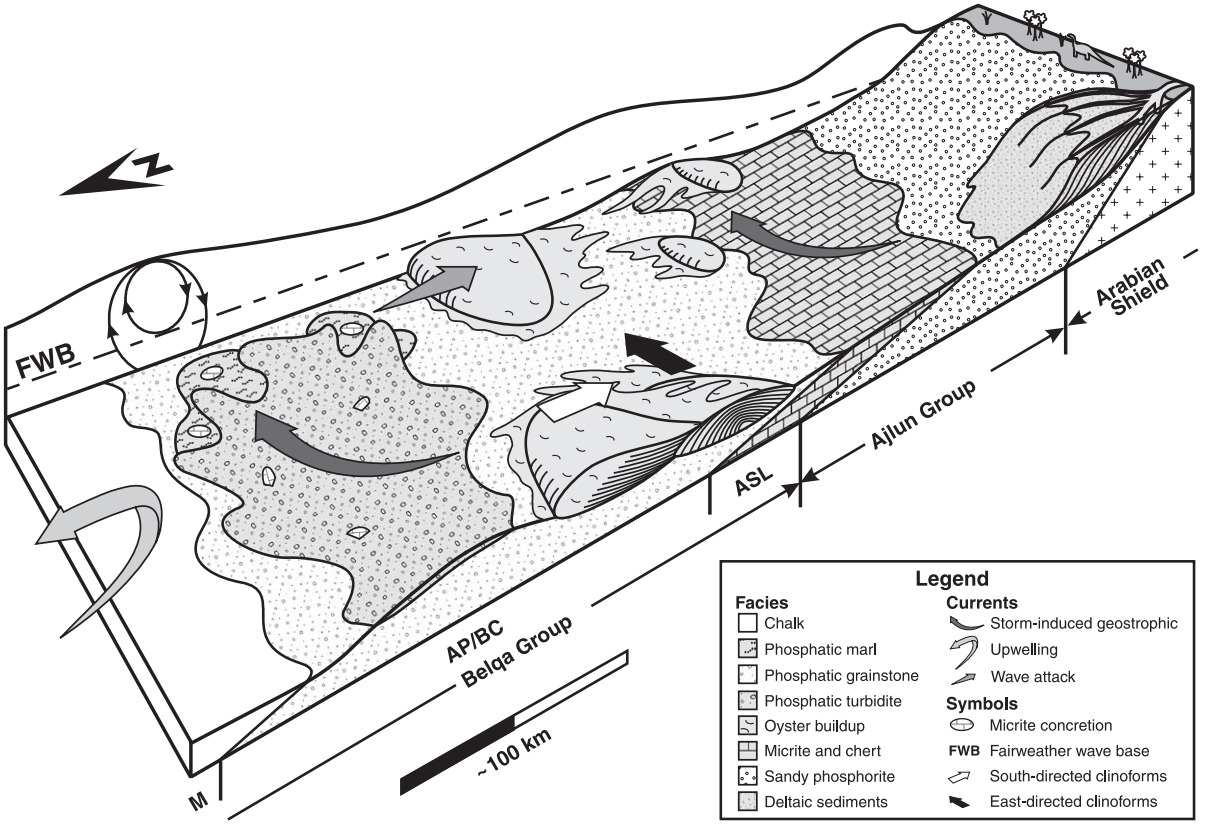

Fig. 7. Paleogeography and current regime during the deposition of the Belqa Group. Refer to text for discussion. The reconstruction of nearshore environments is based on Glenn and Arthur (1990) and Abed and Amireh (1999).

upwelling environments (Barber and Smith, 1981). Here, diatomaceous muds are confined to the middle and inner shelf, whereas organic-rich hemipelagic sediments accumulate farther offshore. These facies belts are diachronous and reflect lateral differences in the planktic ecosystems; the centre and most active parts of the upwelling systems are dominated by diatoms, whereas the margins are dominated by calcareous nannoplankton and autotrophic dinoflagellates (Raymont, 1980). By analogy, the ASL corresponds to the diatom-rich belt, the M corresponds to the lower nutrient nannofossil-rich belt, and the AP records stratigraphic condensation and phosphorite formation in the transitional area between these regions during a rise in relative sea level. Similar conclusions have been reached by Reiss (1988) and Amolgi-Labin et al. (1993) for analogous stratigraphic relations within correlative units from Israel.

We concur with Glenn and Mansour (1979), Reiss (1988), and Kolodny and Garrison (1994) that the major source of P for the STPP was from upwelled waters derived from the Tethyan trough to the north. The paleolatitude of this region was at 10–15°N during the Upper Cretaceous (Hay et al., 1999) and northeast trade winds may have caused the northwest-directed Ekman transport of surface waters that drove coastal upwelling. Kolodny (1980) has suggested that another source of P may have been from riverine input to the south. Glenn and Arthur (1990) have also interpreted correlative phosphorites from the Duwi Group to have formed in shallow water settings in association with prograding deltas, and have postulated that fluvially derived P was important for their formation. However, paleobotanical data from the Kurnub Group in Egypt indicating dry conditions (Wolfe and Upchurch, 1987), the presence of gypsum within Campanian cherts from Israel (Steinitz, 1977) and the peritidal carbonates of the Ajlun Group (Bender, 1974; Powell, 1989), and climate models (Poulsen et al., 1999) suggest that this region was characterized by highly seasonal rainfall and situated at the transition between the tropical and semidesert climatic belts during the Cretaceous (Upchurch et al., 1999). Based on this data and the fact that interbedded siliclastics are conspicuously absent in the ASL, AP, and M we conclude that upwelling was the primary source of P for the phosphorites in central and northern Jordan. On modern shelves surface waters are also rapidly depleted in nutrients away from rivers, and productivity is greatly diminished within relatively short distances from the river mouth (Kennedy, 1984). It is therefore unlikely that river-derived P was transported across the platform into distal environments where phosphogenesis was occurring.

The lack of tidally generated sedimentary structures (Bender, 1974; Powell, 1989; Abed and Amireh, 1999) indicates that the Jordanian shelf had a low tidal range, suggesting that tidal currents played a minimal role in transporting and redistributing sediment. The presence of hummocky cross-stratified grainstones and grainstone/coquina-filled scours, the occurrence of bioclastic carbonates containing shallow water faunas in hemipelagic environments, and the presence of reworked hardgrounds within the ASL and AP indicate episodes of intense storm activity (Aigner, 1985; Einsele and Seilacher, 1991). Considering the abundant evidence for storms we also interpret the *parallel bedded grainstones* and graded oyster coquina beds to be storm generated event beds. These observations are in keeping with other investigations of epeiric systems that have concluded tidal currents were damped in epeiric seas by friction effects operating over the very extensive shallow seafloor, and that the dominant processes affecting epeiric platform sedimentation are the frequency, direction, duration, and magnitude of storms (e.g., Tucker and Wright, 1990 and references therein).

The oyster buildups are similar to other Upper Cretaceous and Cenozoic oyster buildups that dominate (brackish/hypersaline) highly productive tropical marine environments. The enormous size, limited species diversity, and rapid community growth observed within banks and bioherms is attributable to reduced competition for space and nutrients (Glenn and Arthur, 1990). The east to south shift in paleocurrent directions within composite oyster banks is interpreted to record the onlapping of southerly prograding oyster banks over easterly prograding buildups that formed in more proximal shelf positions (Fig. 7). This facies relation indicates that south-directed banks developed in more distal environments and prograded landward during continued sea level rise through the attack of onshore-directed storm and fair-weather waves. We postulate that the dissipation of wave energy on south-directed banks was sufficient to preclude wave-induced progradation of oyster build-

ups developing behind these distal banks in shallower environments. We suggest that progradation of east-directed buildups was driven by storm-generated geostrophic currents that flowed towards the east, parallel to the platform margin. Buildup development ceased when the rate of sea level rise outpaced that of carbonate production and aggradation, effectively stranding oyster buildups on the shelf and eventually blanketing them with chalk.

Geostrophic currents form in response to strong storm winds that drive surface waters onshore producing an ocean surface that is higher at the coast than offshore (Snedden et al., 1988; Duke, 1990). This coastal set-up can be augmented by very low atmospheric pressures and results in a horizontal pressure gradient that acts to drive bottom water offshore. The Coriolis force acts to change the path of the bottom return flow to the right in the northern hemisphere and to the left in the southern hemisphere. Ultimately, a balance between the pressure gradient force and the Coriolis force is achieved when the trajectory of the bottom return flow parallels the shoreline and ceases to accelerate. Direct measurements in the Gulf of Mexico during the passage of hurricanes and tropical storms indicate that geostrophic currents are powerful, and can achieve velocities of 100–200 cm/s (Forristall et al., 1977; Morton, 1981; Snedden et al., 1988). The flow of geostrophic currents is a continuous response to the pressure gradient, and is not a sudden surge of water related to the end of the storm. We hypothesize that powerful geostrophic currents could have developed along the south Tethyan margin in response to strong south-directed storm winds and coastal set-up. The resultant bottom return flow would have been deflected to the east generating a sustained, east-directed, shelf-parallel current competent enough to transport shell material and redistribute sediment along the south Tethyan margin.

Phosphogenesis in the study area was stimulated by the production of pore water phosphate within the upper few centimetres of sediment generated through the microbial respiration of sedimentary organic matter derived from a highly productive surface ocean. The general lack of bioturbation and the presence of benthic foraminifera tolerant of low oxygen conditions within *phosphatic marls*, and $\delta^{13}C$ values from phosphatic peloids indicative of precipitation within the zone of sulfate reduction, all suggest that bottom waters were oxygen deficient, possibly due to the impingement of an oxygen minimum zone (OMZ) on the platform during the accumulation of pristine phosphate (Fig. 8). Facies relations indicate that phosphogenesis along the south Tethyan margin in Jordan was characterized by CFA precipitation in sedimentary environments spanning the entire shelf, wherever the conditions were suitable for phosphogenesis (Bender, 1974; Abed and Al-Agha, 1989; Powell, 1989; Abed and Sadaqah, 1998; Abed and Amireh, 1999; Sadaqah, 2000). This "phosphorite nursery" is a non-uniformitarian phenomenon reflecting phosphate precipitation across a broad depositional spectrum.

Phosphatic grainstones formed through the successive winnowing, transport and redeposition of phosphatic grains and intraclasts derived from pristine phosphate facies via storm-generated currents (Fig. 8). Economic phosphorites were produced through the event-driven amalgamation of the *parallel bedded grainstones* during periods of heightened storm activity. We suggest, based on sedimentologic evidence that indicates the majority of *parallel bedded phosphatic grainstones* were deposited from sustained, turbulent currents as an aggrading traction carpet, the presence of HCS, pot scours, erosive bases to beds, redeposited and broken carbonate concretions, and the preponderance of east-directed oyster buildups, that storm-generated geostrophic currents winnowed and reworked pristine phosphates into granular phosphorite beds. The conspicuous absence of oyster shells within granular phosphorite beds also supports this interpretation and indicates that phosphogenesis and storm transport/amalgamation of phosphatic grainstones occurred contemporaneously in closely adjacent settings. Sediment bypassing across facies belts was evidently not an important mechanism for forming economic phosphorite.

6.3. Marine transgressions and economic phosphorite

The temporal and spatial distribution of phosphorite giants such as the STPP in the Phanerozoic is associated with marine transgressions and has been attributed to extremes in the climatic states of the Earth, causing an accelerated P withdrawal from the ocean into marginal seas and epeiric platforms (Cook and McElhinny, 1979; Arthur and Jenkyns, 1980;

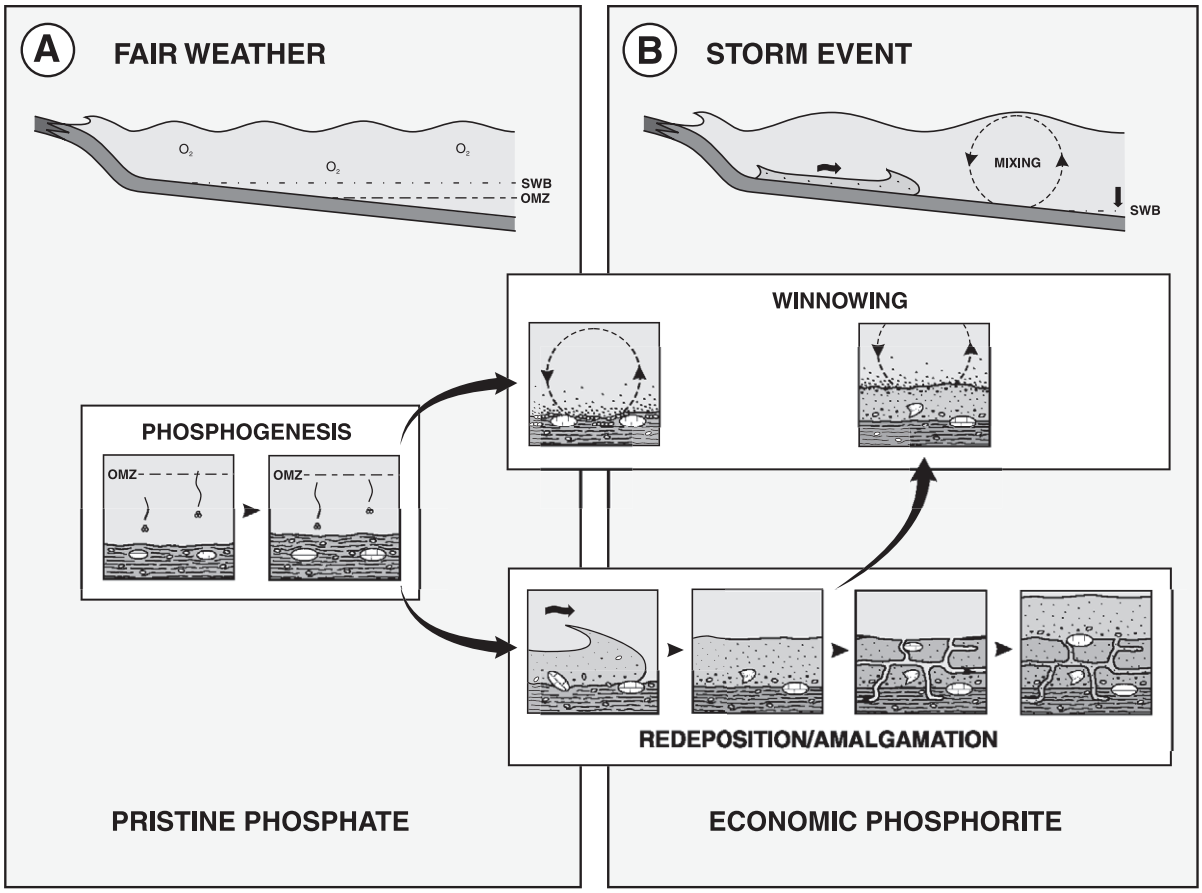

Fig. 8. Depositional model for the formation of economic phosphorite. (A) Pristine phosphate forms during "fairweather" periods under a stratified water column with a well developed oxygen minimum (OMZ) and a shallow storm-weather wave base (SWB). Phosphogenesis is stimulated by high surface productivity and relative stratigraphic condensation. (B) With an increase in storm frequency and intensity with time, the SWB deepens and destratifies the water column. Economic phosphorites form through the amalgamation of storm-induced event beds derived from pristine phosphate facies. Both pristine phosphate facies and the tops of economic phosphorite beds may undergo storm wave winnowing during storm events.

Sheldon, 1980; Glenn et al., 1994), and/or local sedimentologic and tectonic controls on P burial and hydraulic concentration processes (Baturin, 1971; Filippelli and Delaney, 1994). Föllmi et al. (1993, 1994) have demonstrated, based on the correlation of global positive excursions in the pelagic $\delta^{13}C$ record with the deposition of Valanginian, Aptian-Albian, and Miocene phosphorites, that times of increased P deposition are linked to episodes of substantially increased atmospheric carbon dioxide and enhanced carbon burial. As an essential nutrient for life, P governs the biologic productivity on Earth and thus controls the rate at which carbon dioxide is removed from the atmosphere and is converted into organic matter (Föllmi et al., 1993; Föllmi1, 1996; Delaney, 1998; Compton et al., 2000). During an accelerated carbon cycle, atmospheric carbon dioxide levels rise, propelling the Earth into a greenhouse state, in which an evolving warm and humid global climate causes precipitation, runoff, and weathering rates to increase. This, in turn, induces an increase in continental weathering rates and P input into the oceans that may initiate the following chain of negative feedback to cool the Earth's climate: increase in atmospheric carbon dioxide, global warming, enhanced greenhouse conditions → sea level rise, accelerated hydro-

logic cycle, and increased continental weathering → increase in primary production → increased burial of organic matter and increased phosphogenesis → lowering of atmospheric carbon dioxide, weakened greenhouse conditions, global cooling. These periods are associated with increased rates of input of primordial carbon dioxide to the atmosphere from persistent volcanic activity associated with rifting and/or short periods of flood-basalt volcanism (see Föllmi et al., 1993, 1994 for a more complete discussion of this topic). It appears that when the P cycle becomes accelerated during these times, conditions may favour phosphorite formation. As sea level rises in response to an increase in the volume of mid-oceanic ridges, there is a concomitant increase in the accommodation volume on continental shelves, expanding the number of suitable sites for phosphorite accumulation and increased upwelling into midshelf and nearshore areas (Glenn et al., 1994).

Föllmi et al. (1993) has proposed that the Upper Cretaceous STPP records phosphorite deposition during an accelerated P cycle. General Circulation Models show that the Campanian had a warm climate (Frakes, 1999) as a result of significantly higher atmospheric carbon dioxide levels (about 4.4 times greater than today) (Hay and DeConto, 1999). Rampino and Stothers (1988) identified the Late Cretaceous as a period of increased flood-basalt activity, and Föllmi et al. (1993) have recognized significant positive $\delta^{13}C$ excursions in carbonates that correspond to major episodes of phosphorite accumulation along the south Tethyan margin, the southeastern United States, and Mexico. This interpretation is supported by stable oxygen isotopic data from foraminifera, ammonites, belemnites, nautiloids, and mollusks that indicate the Maastrichtian was appreciably cooler than the Campanian (possibly by as much as 3–4 °C) (Frakes, 1999; Barrera and Savin, 1999), suggesting that the Maastrichtian may record the onset of weakened greenhouse conditions associated with the draw down of atmospheric carbon dioxide into the ocean. This interpretation is further substantiated by stratigraphic data from this study that indicate phosphatic strata in Jordan were deposited during a major rise in sea level. This transgression is recognized throughout the eastern Mediterranean and is thought to be associated with the reconfiguration of mid-oceanic ridges during the break-up of Pangea (Flexer et al., 1986; Powell, 1989; Compton et al., 2000). In Jordan this ocean-wide transgression began with the deposition of peritidal carbonates and cherts of the Ajlun Group in the late Albian and continued into the Eocene with the accumulation of hemipelagic carbonates, cherts, and phosphorites of the Belqa Group (Bender, 1974; Powell, 1989).

Aside from the role elevated sea level plays in expanding the accommodation volume on shelves, a rise in relative sea level also favours phosphogenesis by trapping diluting siliciclastics in nearshore environments, and by lowering sediment accumulation rates on shelves (Föllmi, 1990, 1996; Glenn et al., 1994; Taylor and Macquaker, 2000). This relationship between relative sea level rise and stratigraphic condensation also controlled phosphogenesis across the Jordanian shelf.

Marine transgressions also permit wave-induced and other currents to develop along the flooded margin that winnow and rework phosphatic sediments into economic phosphorite (Glenn et al., 1994). In Jordan, storm currents were the most important agent in reworking and concentrating phosphatic sediment into economic phosphorite. The shallow water depths (100–200 m) and large fetches that characterize epeiric seas dramatically increases the area over which storm waves may build and interact with the sea floor (Tucker and Wright, 1990), thus permitting the winnowing and reworking of phosphatic strata across large portions of the platform. This differs significantly from modern shelves whose steeper slopes restrict the zone of wave abrasion (to ~ 70 m water depth) to nearshore environments (James et al., 1992; Boreen and James, 1995).

Unlike previous studies that outline the importance of storm-driven amalgamation of single surge high density phosphatic turbidites to produce thick economic phosphorites (Föllmi and Grimm, 1990; Grimm and Föllmi, 1994), we suggest that sustained turbulent currents generated under storm-induced geostrophic flow are also important in forming economic phosphorite deposits. Geostrophic currents operate for the entire duration of a storm and are capable of reworking, winnowing, and transporting sediment over large areas on modern shelves. We propose that the high current velocities and the long duration over which these shore parallel currents operate make them

very effective agents in reworking and concentrating pristine phosphate facies into economic deposits on storm dominated epeiric platforms. Phosphogenesis and event redeposition however, are insufficient by themselves to form economic phosphorite. Large storms must also be closely spaced in time to produce thick amalgamated deposits.

Syndepositional phosphogenesis, reworking and amalgamation to form economic phosphorite in a single transgressive systems tract contrasts sharply with the principles of ''Baturin Cycling'' for the origin of phosphorites (Baturin, 1971). ''Baturin Cycling'' is widely cited as a mechanism for forming economic phosphorites and relies on major changes in relative sea level to drive the formation of economic phosphorite. In ''Baturin Cycling'' sea level highstands are thought to promote phosphogenesis by increasing the accommodation volume on the shelf. Whereas a lowering of wave base during a fall or low stand in relative sea level is suggested to aid in the reworking and concentration of phosphatic strata into economic phosphorite.

Our model does not necessitate major rises and falls in relative sea level to produce economic phosphorite, but emphasizes the interplay of both auto- and allocyclic sedimentary processes to form phosphatic strata within a single systems tract. Two lines of evidence support our interpretation over ''Baturin Cycling''. First, the vertical stacking pattern of the ASL, AP, and M formations indicates that phosphatic and associated strata in Jordan form a conformable sedimentary succession deposited during a rise in relative sea level. If the economic phosphorite formed through ''Baturin Cycling'' laterally continuous bounding discontinuities reflecting changes in relative sea level would punctuate the stratigraphy. Second, lithofacies associations indicate that pristine phosphate and reworked/event redeposited economic phosphorites are contemporaneous facies. In ''Baturin Cycling'' syndepositional phosphogenesis and reworking of phosphatic strata into economic phosphorites are discrete phenomena separated by a drop in relative sea level, and are thus not contemporaneous. We therefore reject ''Baturin Cycling'' as a plausible model for the formation of economic phosphorite in Jordan because there is no sedimentologic evidence indicating that episodes of phosphogenesis and the subsequent reworking of pristine phosphate into economic phosphorite are discretely separated in time. In our model a transgressive systems tract coupled with high surface productivity created detritally starved settings that were favourable for phosphogenesis, storm reworking of pristine phosphate facies produced granular phosphorite, and amalgamation of storm-generated granular event beds that were closely spaced in time formed economic phosphorite within a transgressive systems tract.

7. Conclusions

(1) The Alhisa Phosphorite Formation forms the upper portion of a TST that was deposited over the peritidal carbonates of the Ajlun Group. These phosphatic sediments are a condensed stratigraphy associated with a rise in relative sea level that culminated with the widespread deposition of pelagic chalk.

(2) Economic phosphorites in Jordan were deposited on a storm-dominated, mixed carbonate-phosphorite epeiric platform along the south Tethyan margin. Sharply based tabular amalgamated beds of massive, normally graded, and indistinctly stratified layers of intraclastic phosphorite are interpreted as granular event deposits. The preponderance of redeposited bored concretions, coquinas containing shallow water faunas in hemipelgaic environments, and hummocky cross stratified phosphatic grainstones indicates episodes of intense storm activity. Chalks record background sedimentation over the platform.

(3) The south Tethyan margin in Jordan was characterized by phosphogenesis in sedimentary environments spanning nearshore, mid-shelf, and distal shelf settings. This ''phosphorite nursery'' is a non-uniformitarian phenomenon reflecting phosphate precipitation across a broad paleoenvironmental spectrum.

(4) Phosphogenesis on the Jordanian shelf was stimulated primarily by the microbial respiration of sedimentary organic matter. Productive surface waters and the export of organic matter to the sediment–water interface created a suboxic seafloor and the necessary solution and surface chemistries for phosphogenesis, probably through the microbial degradation of organic carbon and dissolution of

fish bones and teeth. The lack of any association of pristine phosphate with Fe-bearing authigenic minerals and interbedded siliclastic sediments suggests that iron redox pumping of pore water phosphate played a minimal role in phosphogenesis.

(5) Event-driven amalgamation of phosphatic grainstones derived from pristine phosphate facies produced the economic phosphorites. Amalgamated beds formed by the successive winnowing, transport and redeposition of phosphatic grains from pristine facies via storm-generated single-surge high density turbidity currents, and sustained, highly competent geostrophic currents.

(6) Pristine phosphates, phosphatic event strata, and thick amalgamated economic phosphorites are intimately interbedded in a conformable succession indicating that they were deposited as a mosaic of contemporaneous facies. Syndepositional phosphogenesis and amalgamation to form economic phosphorites contrasts sharply with the principles of ''Baturin Cycling'' for the origin of phosphorites. Our model does not necessitate major rises and falls in relative sea level to produce economic phosphorites, but emphasizes the interplay of both auto- and allocyclic sedimentary processes to form phosphatic strata. A TST coupled with high surface productivity creates detritally starved settings that are favourable for phosphogenesis; storm reworking of pristine phosphate facies produces granular phosphorite; and amalgamation of storm-generated granular event beds forms economic phosphorite within a single systems tract. Our data is consistent with an interpretation that an increase in storm frequency and intensity with time may have been a prerequisite for the formation of economic phosphorite.

The paleoenvironmental reconstructions of the phosphatic and associated facies in Jordan provide a stratigraphic and genetic foundation for other studies in the STPP. Future studies that correlate phosphatic and associated strata from regions surrounding Jordan would further refine interpretations of paleoenvironment and depositional settings. Such a comprehensive study is a prerequisite to fully understanding the auto- and allocyclic processes that governed the environmental evolution, phosphogenesis and the formation of economic phosphorite along the south Tethyan margin.

Acknowledgements

PP gratefully acknowledges Abu Amamdoo, Abu Ismael, Abu Dayub, and Sharkil for their assistance while in the field. J.W. Haggart, E. Thomas, B. Huber, K. Von Salis, F. Jorrisen, and J. Fenner kindly assisted with fossil identification. An early version of the manuscript was read by S.E. Calvert, L.A. Groat, and J.K. Mortensen. This paper was greatly improved by reviews by B.W. Sellwood, R.E. Garrison, and C.J. Poulsen. NSERC provided funding to PP through an operating grant to KG and a postgraduate scholarship. Field work was funded in part by a Geological Association of America Grant (6116-97) and the Society of Economic Geologists Foundation through a Hugh Exton McKinstry Grant. This research was also supported by a University Graduate Fellowship from the University of British Columbia and Killam Predoctoral Fellowships to PP.

References

Abed, A.M., 1988. Eleventh International Field Workshop and Symposium—Guidebook. Third Jordanian Geological Conference International Geological Correlation Program Project 156-Phosphorites (124 pp.).

Abed, A.M., Al-Agha, M.R., 1989. Petrography, geochemistry and origin of the NW Jordan phosphorites. Journal of the Geological Society of London 146, 499–506.

Abed, A.M., Amireh, B.S., 1999. Sedimentology, geochemistry, economic potential and palaeogeography of an Upper Cretaceous phosphorite belt in the southeastern desert of Jordan. Cretaceous Research 20, 119–133.

Abed, A.M., Sadaqah, R., 1998. Role of Upper Cretaceous oyster bioherms in the deposition and accumulation of high-grade phosphorites in Central Jordan. Journal of Sedimentary Research 68, 1009–1020.

Aigner, T., 1985. Storm Depositional System. Springer-Verlag, Berlin. 124 pp.

Al-Bassam, K.S., Al-Dahan, A.A., Jamil, A.K., 1983. Campanian–Maastrichtian phosphorite of Iraq—petrology, geochemistry, and genesis. Mineralium Deposita 18, 215–233.

Almogi-Labin, A., Sass, E., 1990. Agglutinated foraminifera in organic-rich neritic carbonate (Upper Cretaceous, Israel) and their use in identifying oxygen levels in oxygen-poor environments. In: Hemleben, C. et al. (Eds.), Paleoecology, Biostratigraphy, Paleoceanography and Taxonomy of Agglutinated Foraminifera. Kluwer Academic Publishers, Amsterdam, pp. 565–585.

Almogi-Labin, A., Bein, A., Sass, E., 1993. Late Cretaceous upwelling system along the southern Tethys margin (Israel): interrelationship between productivity, bottom water environ-

ments, and organic matter preservation. Paleoceanography 8, 671–690.
Arthur, M.A., Jenkyns, 1980. Phosphorites and paleoceanography. 26th International Geological Congress, Geology of Oceans Symposium, pp. 83–96.
Baker, P.A., Burns, S.J., 1985. Occurrence and formation of dolomite in organic-rich continental margin sediments. AAPG Bulletin 69, 1917–1930.
Baker, P.A., Kastner, M., 1981. Constraints on the formation of sedimentary dolomite. Science 213, 214–216.
Barber, R.T., Smith, R.L., 1981. Coastal upwelling ecosystems. In: Longhurst, A.R. (Ed.), Analysis of Marine Ecosystems. Academic Press, New York, pp. 31–68.
Barrera, E., Savin, S.M., 1999. Evolution of the Late Campanian–Maastrichtian marine climates and oceans. In: Barrera, E., Johnson, C.C. (Eds.), Evolution of the Cretaceous ocean–climate system. Geological Society of America, Boulder, pp. 245–282.
Baturin, G.N., 1971. Stages of phosphorite formation on the ocean floor. Nature 232, 61–62.
Behl, R.J., Garrison, R.E., 1994. The origin of chert in the Monterey Formation of California (USA). In: Iijima, A., Abed, Garrison, R.E. (Eds.), Siliceous phosphatic and glauconitic sediments of the Tertiary and Mesozoic. Proceedings of the 29th International Geological Congress. VSP, Utrecht, pp. 101–132.
Ben-Avraham, Z., 1989. Multiple opening and closing of the eastern Mediterranean and South China Basins. Tectonics 8, 351–362.
Bender, F., 1974. Geology of Jordan. Gebrueder Borntraeger, Berlin. 196 pp.
Benmore, R.A., Coleman, M.L., McArthur, J.M., 1983. Origin of sedimentary francolite from its sulphur and carbon isotope composition. Nature 302, 516–518.
Boreen, T.D., James, N.P., 1995. Stratigraphic sedimentology of Tertiary cool-water limestones, SE Australia. Journal of Sedimentary Research 65, 142–159.
Burnett, W.C., 1977. Geochemistry and origin of phosphorite deposits from off Peru and Chile. Geological Society of America Bulletin 88, 813–823.
Calvert, S.E., 1974. Deposition and diagenesis of silica in marine sediments. Special Publication of the International Association of Sedimentologists, vol. 1. Blackwell Scientific, Oxford, pp. 273–299.
Compton, J.S., Siever, R., 1986. Diffusion and mass balance of Mg during early dolomite formation, Monterey Formation. Geochimica et Cosmochimica Acta 50, 125–135.
Compton, J.S., Hodell, D.A., Garrido, J.R., Mallinson, D.J., 1993. Origin and age of phosphorite from the south-central Florida Platform; relation of phosphogenesis to sea level fluctuations and delta ^{13}C excursions. Geochimica et Cosmochimica Acta 57, 131–146.
Compton, J.S., Donald, H.L., Mallinson, D.J., Hodell, D.A., 1994. Origin of dolomite in the phosphatic Miocene Hawthorn Group of Florida. Journal of Sedimentary Research 64, 638–649.
Compton, J., Mallinson, D., Glenn, C.R., Filippelli, G., Follmi, K., Shields, G., Zanin, Y., 2000. Variations in the global P cycle. In: Glenn, C.R., Prevot-Lucas, L., Lucas, J. (Eds.), Marine Authigenesis: from Global to Microbial. SEPM Special Publication, vol. 66. SEPM, Tulsa, pp. 21–33.
Cook, P.J., McElhinny, M.W., 1979. A re-evaluation of the spatial and temporal distribution of sedimentary phosphate deposits in light of plate tectonics. Economic Geology 74, 315–330.
Delaney, M.L., 1998. P accumulation in marine sediments and the oceanic P cycle. Global Biogeochemical Cycles 12, 563–572.
Donovan, R.N., Foster, R.J., 1972. Subaqueous shrinkage cracks from the Caithness Flagstone Series (Middle Devonian) of northeast Scotland. Journal of Sedimentary Petrology 42, 309–317.
Dott, R.H., Bourgeois, J., 1982. Hummocky stratification: significance of its variable bedding sequences. Geological Society of America Bulletin 93, 663–680.
Duke, W.L., 1990. Geostrophic currents or shallow marine turbidity currents? The dilemma of paleoflow patterns in storm-influenced prograding shoreline systems. Journal of Sedimentary Petrology 60, 870–883.
Duke, W.L., Arnott, R.W.C., Cheel, R.J., 1991. Shelf sandstones and hummocky cross-stratification: new insights on a stormy debate. Geology 19, 625–628.
Einsele, G., Seilacher, A., 1991. Distinction of Tempestites and Turbidites. In: Einsele, G., Ricken, W., Seilacher, A. (Eds.), Cycles and Events in Stratigraphy. Springer-Verlag, Berlin, pp. 377–382.
El-Kammar, A.M., Zayed, M.A., Amer, S.A., 1979. Rare earths of the Nile Valley phosphorites, Upper Egypt. Chemical Geology 24, 69–81.
Filippelli, G.M., Delaney, M.L., 1994. The oceanic P cycle and continental weathering during the Neogene. Paleoceanography 9, 643–652.
Flexer, A., Rosenfeld, A., Lipson, B., Honigstein, A., 1986. Relative sea level changes during the Cretaceous in Israel. AAPG Bulletin 70, 1685–1699.
Föllmi, K.B., 1990. Condensation and phosphogenesis: examples of the Helvetic mid-Cretaceous (northern Tethyan margin). In: Notholt, A.J.G., Jarvis, I. (Eds.), Phosphorite Research and Development. The Geological Society, Oxford, pp. 237–252.
Föllmi, K.B., 1996. The P cycle, phosphogenesis and marine phosphate-rich deposits. Earth-Science Reviews 40, 55–124.
Föllmi, K.B., Grimm, K.A., 1990. Doomed pioneers: gravity-flow deposition and bioturbation in marine oxygen-deficient environments. Geology 18, 1069–1072.
Föllmi, K.B., Garrison, R.E., Grimm, K.A., 1991. Stratification in phosphatic sediments: illustrations from the Neogene of California. In: Einsele, G., Ricken, W., Seilacher, A. (Eds.), Cycles and Events in Stratigraphy. Springer-Verlag, Berlin, Heidelberg, pp. 492–507.
Föllmi, K.B., Garrison, R.B., Ramirez, P.C., Zambrano-Ortiz, F., Kennedy, W.J., Lehner, B.L., 1992. Cyclic phosphate-rich successions in the upper Cretaceous of Colombia. Palaeogeography, Palaeoclimatology, Palaeoecology 93, 151–182.
Föllmi, K.B., Weissert, H., Lini, A., 1993. Nonlinearities in phosphogenesis and P-carbon coupling and their implications for global change. In: Wollast, R., Mackenzie, F.T., Chou, L. (Eds.), Interactions of C, N, P, and S Biogeochemical Cycles and Global Change. NATO ASI Series. Springer-Verlag, Berlin, pp. 447–474.

Föllmi, K.B., Weissert, H., Bisping, M., Funk, H., 1994. Phosphogenesis, carbon-isotope stratigraphy, and carbonate-platform evolution along the Lower Cretaceous northern Tethyan margin. Geological Society of America Bulletin 106, 729–746.

Forristall, G.Z., Hamilton, R.C., Cardone, V.J., 1977. Continental shelf currents in Tropical Storm Delia: observations and theory. Journal of Physical Oceanography 87, 532–546.

Frakes, L.A., 1999. Estimating the global thermal state from Cretaceous sea surface and continental temperature data. In: Barrera, E., Johnson, C.C. (Eds.), Evolution of the Cretaceous ocean–climate system. Geological Society of America, Boulder, pp. 49–57.

Freund, R., 1965. A model of the structural development of Israel and adjacent areas since Upper Cretaceous times. Geological Magazine 102, 189–205.

Froelich, P.N., Klinkhammer, G.P., Bender, M.L., Luedtke, N.A., Heath, G.R., Cullen, D., Dauphin, P., Hammond, D., Hartman, B., Maynard, V., 1979. Early oxidation of organic matter in pelagic sediments of the eastern equatorial Atlantic: suboxic diagenesis. Geochimica et Cosmochimica Acta 43, 1075–1090.

Froelich, P.N., Bender, M.L., Luedtke, N.A., Heath, G.R., DeVries, T., 1982. The marine P cycle. American Journal of Science 282, 474–511.

Froelich, P.N., Kim, K.H., Jahnke, R., Burnett, W.C., Soutar, A., Deakin, M., 1983. Pore water fluoride in Peru continental margin sediments: uptake from seawater. Geochimica et Cosmochimica Acta 47, 1605–1612.

Froelich, P.N., Arthur, M.A., Burnett, W.C., Deakin, M., Hensley, V., Jahnke, R., Kaul, L., Kim, K.H., Roe, K., Soutar, A., Vathakanon, C., 1988. Early diagenesis of organic matter in Peru continental margin sediments: phosphorite precipitation. Marine Geology 80, 308–343.

Garfunkel, Z., Zak, I., Freund, R., 1981. Active faulting in the Dead Sea rift. Tectonophysics 80, 1–26.

Glenn, C.R., 1990. Depositional sequences of the Duwi, Sibaiya and Phosphate Formations, Egypt; phosphogenesis and glauconization in a Late Cretaceous epeiric sea. In: Notholt, A.J.G., Jarvis, I. (Eds.), Phosphorite Research and Development. Geological Society of London Special Publication, vol. 52. The Geological Society of London, Oxford, pp. 205–222.

Glenn, C.R., Arthur, M.A., 1988. Petrology and major element geochemistry of Peru margin phosphorites and associated diagenetic minerals: authigenesis in modern organic rich sediments. Marine Geology 80, 231–268.

Glenn, C.R., Arthur, M.A., 1990. Anatomy and origin of a Cretaceous phosphorite-greensand giant, Egypt. Sedimentology 37, 123–154.

Glenn, C.R., Mansour, S.E.A., 1979. Reconstruction of the depositional and diagenetic history of phosphorites and associated rocks of the Duwi Formation (Late Cretaceous) Eastern Desert, Egypt. Annals of the Geological Survey of Egypt IX, 388–407.

Glenn, C.R., Föllmi, K.B., Riggs, S.R., Baturin, G.N., Grimm, K.A., Trappe, J., Abed, A.M., Galli-Oliver, C., Garrison, R.E., Ilyin, A.V., Jehl, C., Rohrlich, V., Sadaqah, R.M.Y., Schidlowski, M., Sheldon, R.E., Siegmund, H., 1994. P and phosphorites: sedimentology and environments of formation. Eclogae Geologicae Helvetiae 87, 747–788.

Greenwood, R., 1973. Cristabolite: its relationship to chert formation in selected samples from the Deep Sea Drilling Project. Journal of Sedimentary Petrology 43, 700–708.

Grimm, K.A., 1997. Phosphorites feed people, Farm Folk/City Folk's Newsletter 13, 4–5.

Grimm, K.A., 2000. Stratigraphic condensation and the redeposition of economic phosphorite: allostratigraphy of Oligo-Miocene shelfal sediments, Baja California Sur, Mexico. In: Glenn, C.R., Prevot-Lucas, L., Lucas, J. (Eds.), Marine authigenesis: from global to microbial. SEPM Special Publications. Society for Sedimentary Geology, Tulsa, pp. 325–347.

Grimm, K.A., Föllmi, K.B., 1994. Doomed pioneers: allochthonous crustacean tracemakers in anaerobic basinal strata, Oligo-Miocene San Gregorio Formation, Baja California Sur, Mexico. Palaios 9, 313–334.

Haggart, J.W., 2000, Report on Upper Cretaceous fossils from the Amman Formation, Jordan. Paleontological Report JWH-2000-06, Geological Survey of Canada, Vancouver.

Hay, W.W., DeConto, R.M., 1999. Comparison of modern and Late Cretaceous meridianal energy transport and oceanology. In: Barrera, E., Johnson, C.C. (Eds.), Evolution of the Cretaceous ocean–climate system. Geological Society of America, Boulder, pp. 283–300.

Hay, W.W, DeConto, R.M., Wold, C.N., Wilson, K.M., Voigt, S., Schulz, M., Wold-Rossby, A., Dullo, W.C., Ronov, A.B., Balukhovsky, A.N., Soding, E., 1999. Alternative global Cretaceous paleogeography. In: Barrera, E., Johnson, C.C. (Eds.), Evolution of the Cretaceous Ocean–Climate System. Geological Society of America, Boulder, CO, pp. 1–47.

Heggie, D.T., Skyring, G.W., O'Brien, G.W., Reimers, C., Herczeg, A., Moriarty, D.J.W., Burnett, W.C., Milnes, A.R., 1990. Organic carbon cycling and modern phosphorite formation on the East Australia continental margin: an overview. In: Notholt, A.J.G., Jarvis, I. (Eds.), Phosphorite research and development. The Geological Society of London, Oxford, pp. 87–117.

Hinman, N.W., 1990. Chemical factors influencing the rates and sequences of silica phase transitions: effects of organic constituents. Geochimica et Cosmochimica Acta 54, 1563–1574.

Hiscott, R.N., 1994. Traction-carpet stratification in turbidites—fact or fiction? Journal of Sedimentary Research, A 64, 204–208.

Irwin, H., Curtis, C., Coleman, M., 1977. Isotopic evidence for source of diagenetic carbonates formed during burial of organic-rich sediments. Nature 269, 209–213.

Isaacs, C.M., 1982. Influence on rock composition on kinetics of silica phase changes in the Monterey Formation, Santa Barbara area, California. Geology 10, 304–308.

Jahnke, R.A., Emerson, S.R., Roe, K.K., Burnett, W.C., 1983. The present day formation of apatite in Mexican continental margin sediments. Geochimica et Cosmochimica Acta 47, 259–266.

James, N.P., Bone, Y., van der Borch, C.C., Gostin, V.A., 1992. Modern carbonate and terrigenous clastic sediments on a cool water, high energy, mid-latitude shelf: Lacepe, southern Australia. Sedimentology 39, 877–903.

Jarvis, I., Burnett, W.C., Nathan, Y., Almbaydin, F.S.M., Attia, A.K.M., Castro, L.N., Flicoteaux, R., Hilmy, M.E., Husain, V.,

Quatawnah, A.A., Serjani, A., Zanin, Y.N., 1994. Phosphorite geochemistry: state-of-the-art and environmental concerns. Eclogae Geologicae Helveticae 87, 643–700.

Jasinski, S.M., 2000. Phosphate Rock. U.S. Geological Survey Mineral Commodity Summaries. U.S. Geological Survey (http://minerals.usgs.gov/minerals/pubs/mcs).

Kennedy, V.S., 1984. The Estuary as a Filter. Academic Press, Orlando. 511 pp.

Kolodny, Y., 1967. Lithostratigraphy of the Mishash Formation, Northern Negev. Israel Journal of Earth Sciences 16, 57–73.

Kolodny, Y., 1980. Carbon isotopes and depositional environment of a high productivity sedimentary sequence—the case of the Mishash–Ghareb Formations, Israel. Israel Journal of Earth Sciences 29, 147–156.

Kolodny, Y., Garrison, R.E., 1994. Sedimentation and diagenesis in paleoupwelling zones of epeiric sea and basinal settings: a comparison of the Cretaceous Mishash Formation of Israel and the Miocene Monterey Formation of California. In: Iijima, A., Abed, Garrison, R.E. (Eds.), Siliceous phosphatic and glauconitic sediments of the Tertiary and Mesozoic. Proceedings of the 29th International Geological Congress VSP, Utrecht, pp. 133–158.

Kolodny, Y., Kaplan, I.R., 1970. Carbon and oxygen isotopes in apatite CO_2 and co-existing calcite from sedimentary phosphorite. Journal of Sedimentary Petrology 40, 954–959.

Kolodny, Y., Taraboulos, A., Frieslander, U., 1980. Participation of fresh water in chert diagenesis: evidence from oxygen isotopes and boron track mapping. Sedimentology 27, 305–316.

Lowe, D.R., 1982. Sediment gravity flows: II. Depositional models with special reference to the deposits of high-density turbidity currents. Journal of Sedimentary Petrology 52, 279–297.

MacEachern, J.A., Pemberton, S.G., Raychaudhuri, L., 1992. Stratigraphic applications of the *Glossifungites* ichnofacies: delineating discontinuities in the stratigraphic record. In: Pemberton, S.G. (Ed.), Applications of ichnology to petroleum exploration. SEPM Core Workshop, vol. 17. SEPM, Tulsa, pp. 169–198.

Masri, M., 1963. Report on the geology of the Amman–Zarqa area. Central Water Authority of Jordan, Amman. 74 pp.

McArthur, J.A., Herczeg, A., 1990. Diagenetic stability of the isotopic composition of phosphate oxygen: paleoenvironmental implications. In: Notholt, A.J.G., Jarvis, I. (Eds.), Phosphorite Research and Development. The Geological Society Publishing House, Avon, pp. 119–124.

McArthur, J.M., Coleman, M.L., Bremner, J.M., 1980. Carbon and oxygen isotopic composition of structural carbonate in sedimentary francolite. Journal of the Geological Society of London 137, 669–673.

McArthur, J.M., Benmore, R.A., Coleman, M.L., Soldi, C., Yeh, H.W., O'Brien, G.W., 1986. Stable isotopes characterisation of francolite formation. Earth and Planetary Science Letters 77, 20–34.

McCrea, J.M., 1950. On the isotopic chemistry of carbonates and a palaeotemperature scale. The Journal of Chemical Physics 18, 849–857.

Morton, R.A., 1981. Formation of storm deposits by wind-forced currents in the Gulf of Mexico and the North Sea. In: Nio, S.D., Shuttenhelm, R.T.E., van Weering, T.C.E. (Eds.), Holocene marine sedimentation in the North Sea basin. International Association of Sedimentologists, pp. 385–396.

Myrow, P.M., 1992. Pot and gutter casts from the Chapel Island Formation, southeast Newfoundland. Journal of Sedimentary Petrology 62, 992–1007.

Nathan, Y., Shiloni, Y., Roded, R., Gal, I., Deutsch, Y., 1979. The geochemistry of the northern and central Negev phosphorites (southern Israel). Bulletin of the Israel Geological Survey 34, 1–23.

Nathan, Y., Soudry, D., Levy, Y., Shitrit, D., Dorfman, E., 1997. Geochemistry of cadmium in the Negev phosphorites. Chemical Geology 142, 87–107.

Notholt, A.J.G., 1985. Phosphate resources in the Mediterranean (Tethyan) phosphogenic province: a progress report. Sciences Geologiques. Memoire 77, 9–21.

Notholt, A.J.G., Sheldon, R.P., Davidson, D.F., 1989. Phosphate deposits of the world. Phosphate Rock Resources, vol. 2. Cambridge Univ. Press, Cambridge. 566 pp.

Pedersen, T.E., Calvert, S.E., 1990. Anoxia vs. Productivity: what controls the formation of organic carbon-rich sediments and sedimentary rocks? AAPG Bulletin 74, 456–466.

Pemberton, S.G., Frey, R.W., 1985. The *Glossifungites* ichnofacies: modern examples from the Georgia coast, U.S.A. In: Curran, H.A. (Ed.), Biogenic Structures: Their Use in Interpreting Depositional Environments. SEPM, Tulsa, pp. 237–259.

Poulsen, C.J., Barron, E.J., Johnson, C.C., Fawcett, P., 1999. Links between major climatic factors and regional oceanic circulation in the mid-Cretaceous. In: Barrera, E., Johnson, C.C. (Eds.), Evolution of the Cretaceous ocean–climate system. Geological Society of America, Boulder, CO, pp. 73–89.

Powell, J.H., 1989. Stratigraphy and sedimentation of the Phanerozoic rocks in central and south Jordan. Natural Resources Authority, Geological Mapping Division, Amman. 130 pp.

Pratt, B.R., 1998. Syneresis cracks: subaqueous shrinkage in argillaceous sediments caused by earthquake-induced dewatering. Sedimentary Geology 117, 1–10.

Rampino, M.R., Stothers, R.B., 1988. Flood basalt volcanism during the past 250 million years. Science 241, 663–668.

Raymont, J.E.G., 1980. Plankton and Productivity in the Ocean, Phytoplankton, vol. 1. Pergamon, New York. 489 pp.

Reiss, Z., Almogi-Labin, A., Honigstein, A., Lewy, Z., Lipson-Benitah, S., Moshkovitz, S., Zaks, Y., 1985. Late Cretaceous multiple stratigraphic framework of Israel. Israel Journal of Earth Sciences 34, 147–166.

Reiss, Z., 1988. Assemblages from a Senonian high-productivity sea. Revue de Paleobiologie 2, 323–332 (Special Volume).

Sadaqah, R.M., 2000. Phosphogenesis, Geochemistry, Stable Isotopes and Depositional Sequences of the Upper Cretaceous Phosphorite Formation in Jordan. PhD thesis, University of Jordan, Amman. 257 pp.

Schuffert, J.D., Kastner, M., Jahnke, R.A., 1998. Carbon and P burial associated with modern phosphorite formation. Marine Geology 146, 21–31.

Sheldon, R.P., 1980. Episodicity of phosphate deposition and deep ocean circulation—a hypothesis. In: Bentor, Y.K. (Ed.), Marine Phosphorites—Geochemistry, Occurrence, Genesis. Society of Economic Paleontologists and Mineralogists, pp. 239–247.

Sheldon, R.P., 1981. Ancient marine phosphorites. Annual Review of Earth Planetary Sciences 9, 251–284.

Shemesh, A., Kolodny, Y., Luz, B., 1983. Oxygen isotope variations in phosphate of biogenic apatites: II. Phosphorite rocks. Earth and Planetary Science Letters 64, 405–416.

Silverman, S.R., Fugat, R., Weiser, J.D., 1952. Quantitative determination of calcite associated with carbonate-bearing apatite. American Mineralogist 37, 211–222.

Snedden, J.W., Nummedal, D., Amos, A.F., 1988. Storm- and fair-weather combined flow on the central Texas continental shelf. Journal of Sedimentary Petrology 58, 580–595.

Sohn, Y.K., 1997. On traction-carpet sedimentation. Journal of Sedimentary Research 67, 502–509.

Soudry, D., 1992. Primary bedded phosphorites in the Campanian Mishash Formation, Negev, southern Israel. Sedimentary Geology 80, 77–88.

Soudry, D., Champetier, Y., 1983. Microbial processes in the Negev phosphorites (southern Israel). Sedimentology 30, 411–423.

Soudry, D., Moshkovitz, S., Ehrlich, A., 1981. Occurrence of siliceous microfossils (diatoms, silicoflagellates and sponge spicules) in the Campanian Mishash Formation, southern Israel. Eclogae Geologicae Helveticae 74, 97–107.

Steinitz, G., 1977. Evaporite-chert associations in Senonian bedded cherts, Israel. Israel Journal of Earth-Sciences 26, 55–63.

Suess, E., 1981. Phosphate regeneration from sediments of the Peru Continental margin by dissolution of fish debris. Geochimica et Cosmochimica Acta 45, 577–588.

Taylor, K.G., Macquaker, J.H.S., 2000. Spatial and temporal distribution of authigenic minerals in continental shelf sediments: implications for sequence stratigraphic analysis. In: Glenn, C.R., Prevot-Lucas, L., Lucas, J. (Eds.), Marine Authigenesis: from Global to Microbial. SEPM Special Publication, vol. 66. SEPM, Tulsa, pp. 309–323.

Tsujita, C.J., 1995. Origin of Concretion-Hosted Shell Clusters in the Late Cretaceous Bearpaw Formation, Southern Alberta, vol. 10. Palaios, Canada, pp. 408–423.

Tucker, M.E., Wright, V.P., 1990. Carbonate Sedimentology. Blackwell Scientific Publications, London. 482 pp.

Upchurch, J.G.R., Otto-Bliesner, B.L., Scotese, C.R., 1999. Terrestrial vegetation and its effects on climate during the latest Cretaceous. In: Barrera, E., Johnson, C.C. (Eds.), Evolution of the Cretaceous ocean–climate system. Geological Society of America, Boulder, CO, pp. 407–426.

Wetzel, A., Allia, V., 2000. The significance of hiatus beds in shallow-water mudstones: an example from the Middle Jurassic of Switzerland. Journal of Sedimentary Research 70, 170–180.

Wetzel, R., Morton, D.M., 1959. Contribution a la geologie de la Transjordanie. In: Dubertret, L. (Ed.), Notes et Memoirs sur le Moyen Orient, pp. 95–191.

Widmark, J.G.V., Speijer, R.P., 1997. Benthic foraminiferal faunas and trophic regimes at the terminal Cretaceous Tethyan seafloor. Palaios 12, 354–371.

Wolfe, J.A., Upchurch, G.R., 1987. North American nonmarine climates and vegetation during the Late Cretaceous. Palaeogeography, Palaeoclimatology, Palaeoecology 61, 33–77.

Zijlstra, J.J.P., 1995. The Sedimentology of Chalk, vol. 54. Springer-Verlag, Berlin. 194 pp.